GeoHazards

MDPI

Article

La Palma 2021 Eruption (Canary Islands): Measurements and Modelling of Lava Flow Cooling Rates and Applications for Infrastructure Reconstruction and Risk Mitigation

Luis González-de-Vallejo [1,2,*], Aaron Álvarez-Hernández [1], Mercedes Ferrer [3], John P. Lockwood [4], Nemesio M. Pérez [1,5], Pedro A. Hernández [1,5], Ana Miranda-Hardisson [1], José A. Rodríguez-Losada [1,6], David Afonso-Falcón [5], Héctor de-los-Ríos [5], Javier Páez-Padilla [1] and Luis E. Hernández-Gutiérrez [1,7]

1 Volcanological Institute of the Canary Islands (INVOLCAN), 38400 Puerto de la Cruz, Spain; aalvarez@involcan.org (A.Á.-H.); nperez@iter.es (N.M.P.); amirandahar@gmail.com (A.M.-H.); jrlosada@ull.edu.es (J.A.R.-L.); paezpadilla.javier@gmail.com (J.P.-P.); lhergut@gobiernodecanarias.org (L.E.H.-G.)
2 Department of Geodynamics, Faculty of Geology, Complutense University of Madrid (UCM), 28040 Madrid, Spain
3 Department of Geological Hazards, Geological and Mining Institute of Spain (IGME)—CSIC, 28003 Madrid, Spain; m.ferrer@igme.es
4 Department of Geology, University of Hawaii at Hilo, Hilo, HI 96720, USA; jplockwood1963@outlook.com
5 Institute of Technology and Renewable Energies (ITER), 38600 Granadilla de Abona, Spain; dafonso@iter.es (D.A.-F.); hrios@iter.es (H.d.-l.-R.)
6 Department of Animal Biology, Soil Science and Geology, University of La Laguna (ULL), 38200 San Cristóbal de La Laguna, Spain
7 Department of Public Works, Housing, and Mobility, Government of the Canary Islands (GOBCAN), 38001 Santa Cruz de Tenerife, Spain
* Correspondence: vallejo@ucm.es

Abstract: On 19 September 2021, a strombolian volcanic eruption began on the island of La Palma in the Canary Islands. This event resulted in the destruction of 73 km of roads, urban infrastructure, numerous houses, and agricultural crops, affecting approximately 7200 people and causing losses exceeding 1.2 billion euros. Around 12 km^2 were covered by aa and pahoehoe lava flows, which reached thicknesses of over 70 m. Following the end of the eruption, thermal, geological, and geotechnical site investigations were carried out for the reconstruction and territorial and urban planning, with the main objectives focused on opening roads through hot lava, constructing new urban settlements in areas covered by lava flows, and facilitating the agricultural recovery. The primary challenges to reconstruction included the very slow cooling rate of the lava, resulting in persistent high temperatures, exceeding 500 °C, its highly heterogeneous geotechnical properties with numerous cavities and lava caves, and the presence of toxic gases. Site investigations included geotechnical boreholes, seismic geophysics and ground-penetration radar, and temperature measurements of lava flows using drones and thermocouple devices inside boreholes. To estimate the cooling rates of the lava flows, two physical cooling models were developed based on thermal behavior and geological–geotechnical data. The results indicated that lava cooling durations in some areas exceed practical waiting times for commencing reconstruction. This led to the development of geological engineering solutions that permit road construction and urban and agricultural reconstruction to begin sooner than estimated by the cooling models. On the other hand, potential hazards arising from the eruption process have also been taken into account. Stability analyses of the 200 m high volcanic cone formed during the eruption indicate the possibility of failure in the event of heavy rain and consequently lahar hazards. The results of the investigations carried out and their applications to post-disaster reconstruction may be useful for other volcanic regions, contributing to minimizing risk to infrastructure and urban settlements.

Keywords: La Palma post-eruption reconstruction; lava flows cooling rates; volcanic geohazards

Citation: González-de-Vallejo, L.; Álvarez-Hernández, A.; Ferrer, M.; Lockwood, J.P.; Pérez, N.M.; Hernández, P.A.; Miranda-Hardisson, A.; Rodríguez-Losada, J.A.; Afonso-Falcón, D.; de-los-Ríos, H.; et al. La Palma 2021 Eruption (Canary Islands): Measurements and Modelling of Lava Flow Cooling Rates and Applications for Infrastructure Reconstruction and Risk Mitigation. *GeoHazards* **2024**, *5*, 1093–1124. https://doi.org/10.3390/geohazards5040052

Academic Editor: Dickson Cunningham

Received: 21 July 2024
Revised: 24 September 2024
Accepted: 28 September 2024
Published: 4 October 2024

1. Introduction and Objectives

La Palma, with 706 km^2 in extension and a maximum altitude of 2423 m a.s.l., is the most active volcanic island in the Canary Archipelago according to historical records. It has a roughly triangular shape with a predominant N–S axis, and consists of two main volcanic edifices: an almost hexagonal northern ancient shield formed by the Garafia, Taburiente, and Bejenado volcanoes, dating from 2 to 0.5 Ma ago, and a more recent southern rift zone elongated in a N–S direction known as Cumbre Vieja volcano, with ages ranging from 0.5 Ma to present. Historic eruptions have occurred approximately in 1480 (Tacande), 1585 (Tahuya), 1646 (Tigalate), 1677 (San Antonio), 1712 (El Charco), 1949 (San Juan), 1971 (Teneguía), and 2021 (known as Tajogaite).

Previous historical eruptions along the Cumbre Vieja north–south rift zone have been characterized by the emergence of multiple vents aligned obliquely to the rift zone. Eruptive activity has typically been explosive at the summit vents and effusive at the base and flanks of the volcanoes, producing basaltic lavas, basanites, tephrites, and phonotephrites [1–3].

The eruption of the Tajogaite volcano has had a catastrophic effect on the population residing on the western side of the island [4–6]. The regional and national authorities are collaborating with the scientific community to find solutions to aid recovery of the impacted area in the shortest possible time while ensuring the safety of the population.

One of the main current problems is the lack of knowledge regarding the cooling rate for lava flows of great thicknesses, as observed in the case here studied. Even two years after the end of the eruption, there are still areas where surface or near-surface temperatures remain above 500 °C. This poses a critical obstacle to the recovery and reconstruction efforts. Studies on this subject are scarce [7–14]. On the other hand, cooling mechanisms of lava flows have been considered by [15–17].

The main aim of this study is to evaluate and assess the cooling rates of lava flows, which is a key question for providing engineering solutions for infrastructure reconstruction and territorial planning, as well as implementing post-eruption mitigation measures.

Effects of the Volcanic Eruption

The Tajogaite volcanic eruption occurred on the west side of La Palma near the Cabeza de Vaca trail in the municipality of El Paso, on 19 September 2021 (Figure 1), following 50 years of volcanic quiescence on the island. The eruption lasted for nearly three months, ceasing on 13 December 2021, resulting in the destruction of about 1700 buildings and the displacement of approximately 7000 people.

A total of 73.8 km of roads and 370 Ha of agricultural land were buried by lava flows, and 2988 buildings were affected. Damage to public and private property resulting from the eruption exceeded 842 M euros [18], distributed as follows:

- Damage to roads: 228 M euros.
- Destruction of crops and associated production losses: 200 M euros.
- Destruction of buildings: 165 M euros.

In addition, the eruption has caused economic stagnation in the affected areas, stemming from both material losses and the inability to access workplaces and business centers.

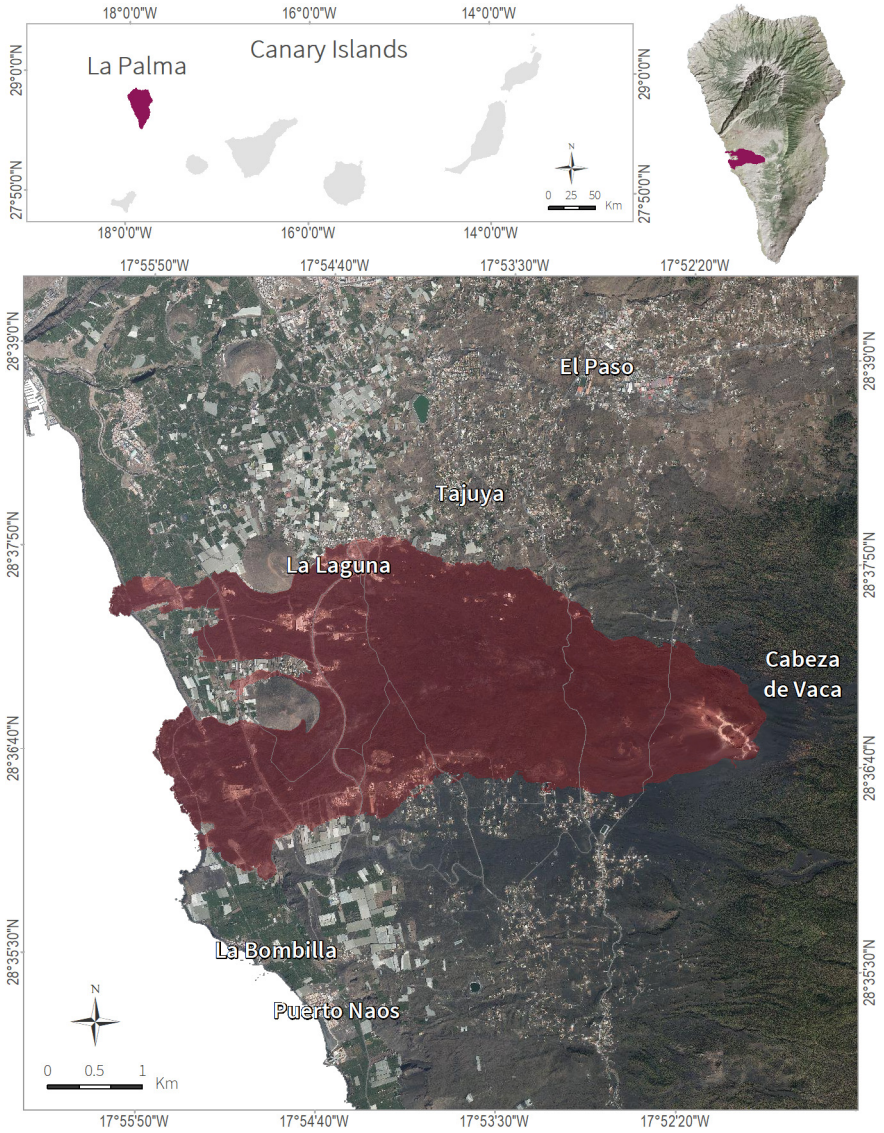

Figure 1. La Palma Island and lava flow field location.

2. Geological Setting and Lava Flows Description

The 2021 eruption was characterized as a fissural basaltic eruption, predominantly exhibiting strombolian activity with occasional phreatomagmatic episodes [4]. The magnitude of the eruption, according to the Volcanic Explosivity Index VEI [19], has been classified as VEI 3 on a scale from 0 to 8 [20].

The total estimated volume of material emitted in the eruption exceeded 200 M m^3. The extensive new lava field formed in the western part of the island covers an area of 1219 Ha. Approximately 67% of the lava reaches thicknesses of up to 15 m, 24% reaches 30 m, 7% reaches 45 m, and roughly 1.2% reaches thicknesses of up to 60 m. The estimated average thickness of the lava is 12 m, with a maximum of over 70 m (see Section 3.1). This volume of lavas accumulated in just 85 days, the duration of the eruption from 19 September to 13 December 2021) (Figure 2).

The two main types of basaltic lavas, aa and pahoehoe, were emitted, with block lavas and accretionary lava balls also identified [21]. Aa lavas predominate over the pahoehoe lavas, and their percentages in surface area (Figure 3) have been estimated: 91.2% aa lavas (10,653,860 m^2) and 8.4% pahoehoe (979,426 m^2). The main characteristics of the two types of lava have been described by [15,22,23]. The Tajogaite lava flows present the following characteristics:

- Aa lavas are formed from magmas with higher viscosity compared to pahoehoe lavas, flow more slowly, and have a markedly different appearance. Their surface is extremely rough or even spiny. A vertical section of aa lava consists of an inner core of dense basalts marked by a network of joints or fissures, formed by contraction as the molten material cools and solidifies; this core is bounded below and above by irregular scoriaceous crusts or bands (Figure 4). When multiple aa lavas stack upon each other, the uppermost layer of scoria mixes with those at the base of the melt immediately above, resulting in an alternation of basalts and scoria autobreccia.
- Pahoehoe lavas are characterized by a smooth and undulating surface, forming cooling ropes (Figure 5). This type of lava contains numerous vesicles and is marked by the presence of volcanic cavities or caves, which can extend kilometers in length with diameters reaching several meters. In situ investigations carried out on these materials have identified several of these volcanic caves (see Section 3.2).

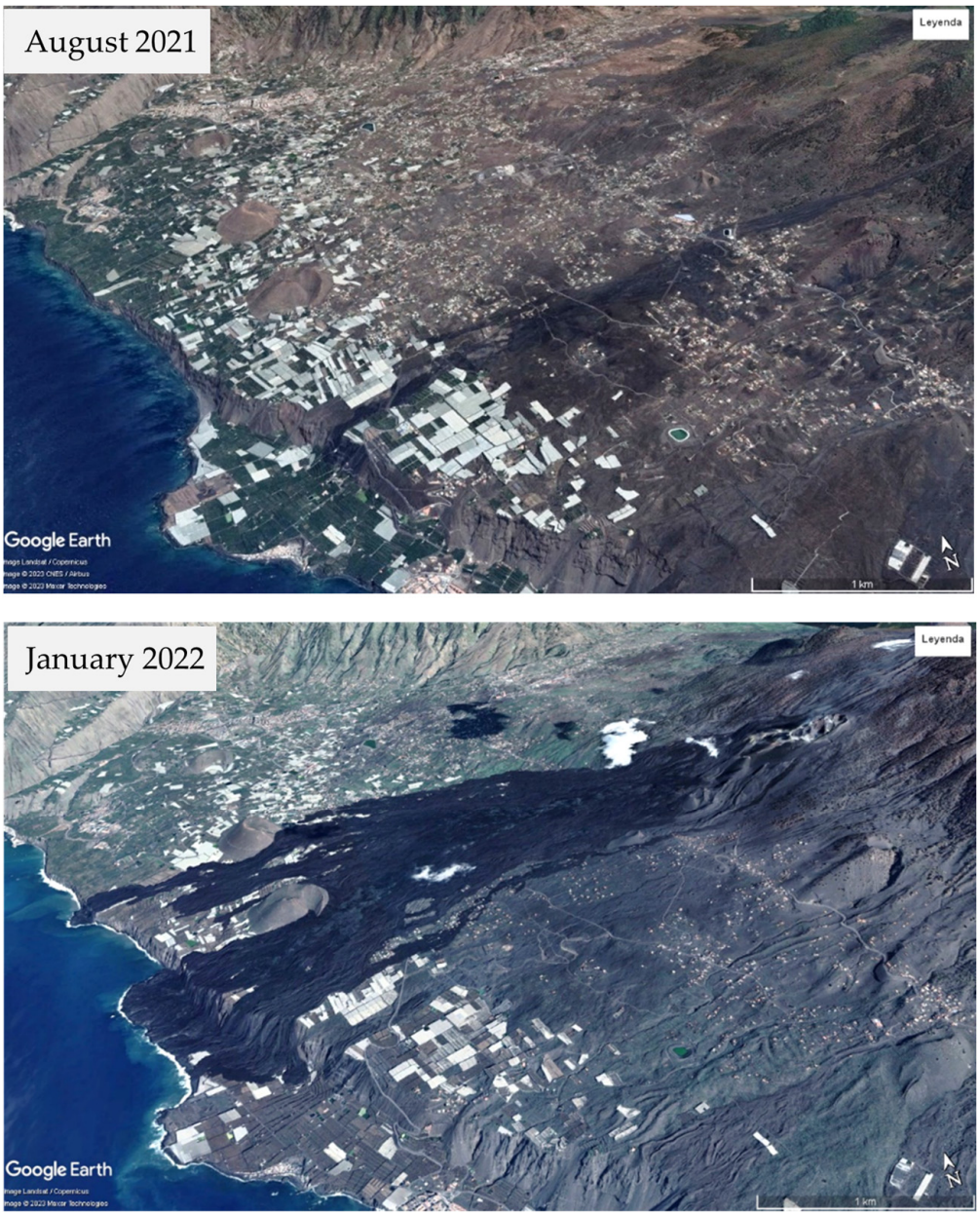

Figure 2. Aerial views before and after the 2021 volcanic eruption (Source: Google Earth).

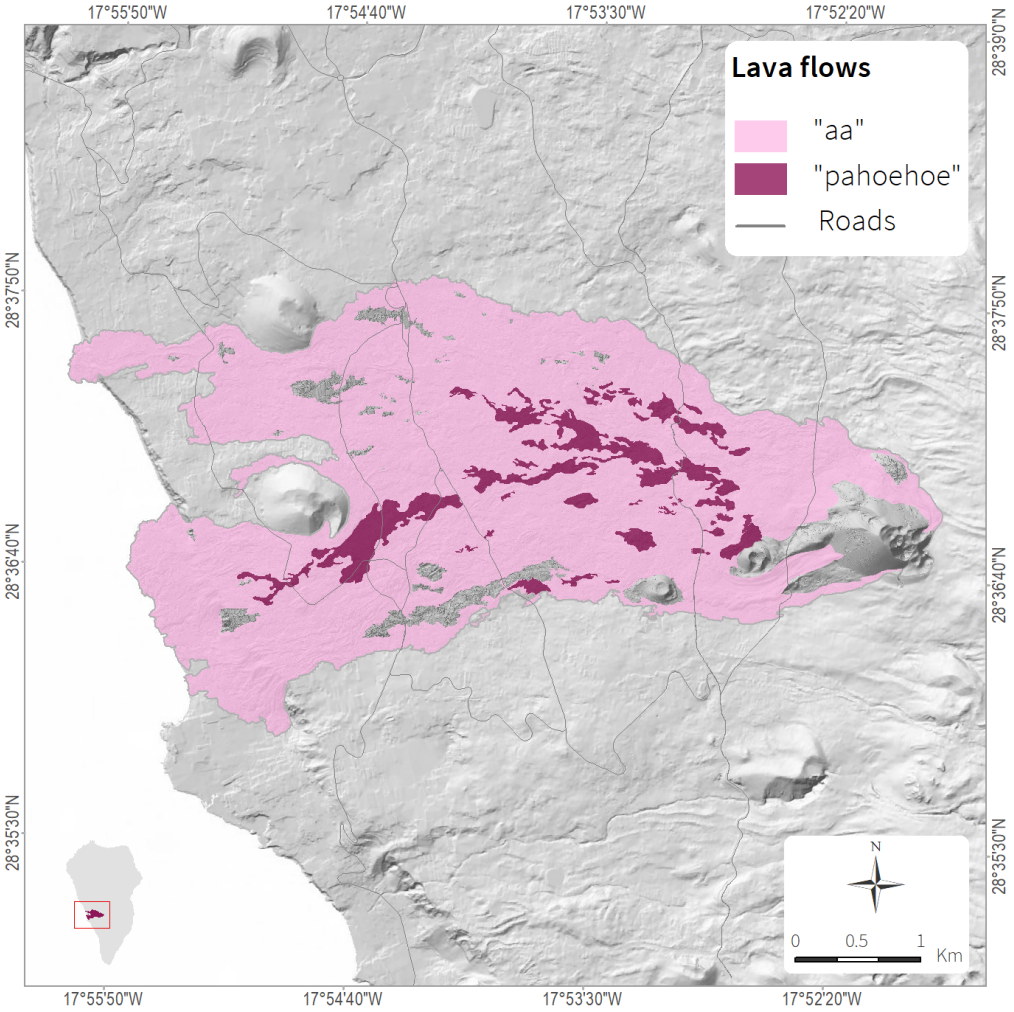

Figure 3. Type of lava flows' distribution from the La Palma 2021 eruption.

Figure 4. Aa lava flow section showing upper and lower scoriaceous crusts (dark brown) surrounding dense aa core (gray). The black point inside the circle indicates the site where the photo was taken on the lava field (see Figure 3).

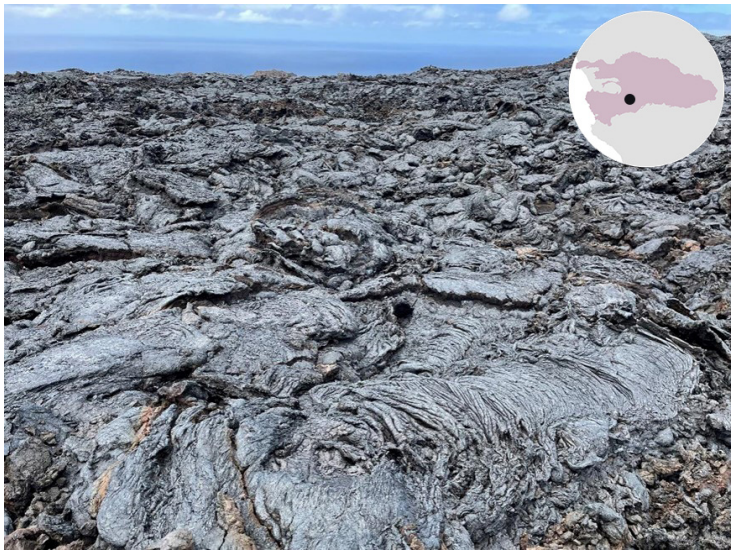

Figure 5. Pahoehoe lava flows showing cooling ropes from the La Palma 2021 eruption. The black point inside the circle indicates the site where the photo was taken on the lava field (see Figure 3).

3. Site Investigations

The scarcity of land for urban development in areas adjacent to the lava flows made it necessary to recover lava-covered areas for urban uses and infrastructural purposes. The high temperatures of the lava flows and the geotechnical characteristics of the lava materials, including the presence of cavities or lava tubes, were decisive factors in this endeavor. To achieve these goals, the following site investigations were conducted.

3.1. Geotechnical Investigations

Four geotechnical rotary boreholes were drilled with continuous core recovery, their locations determined by accessibility (Figures 6 and 7) and the temperatures of the lava flows, which in many areas exceeded 500 °C. The main data from the boreholes are summarized in Table 1. Systematic temperature measurements were taken in the boreholes at various depths from August 2022 to the present (2024). Laboratory tests were conducted on the samples obtained to determine specific weight, strength, cohesion, internal friction angle, and grain size distribution.

Table 1. Summary of borehole data.

Borehole No.	Depth (m)	Thickness (m)	Lithology	T °C	Borehole Length (m)	Lava Flow Thickness (m)
S-1	0.14 1.4–4.0 4.0–10.3	1.4 2.6 6.3	Lava scoria Massive basalt Lava scoria	284°	10.3	10.9
S-2	0.0–1.1 1.1–2.5	1.1 1.4	Lava scoria Massive basalt	240°	2.5	10.9
S-3	0.0–0.5 0.5–2.2 2.2–5.6 5.6–7.6	0.5 1.7 3.4 2.0	Lava scoria Massive basalt Lava scoria Massive basalt	120°	7.6	14.8
S-4	0.0–0.80 0.80–3.0 3.00–5.05	0.80 2.20 2.05	Massive basalt Cavity Lava scoria	551°	5.0	22.1

Temperatures measured at a depth of 2 m inside boreholes, August 2022. See Figure 6 for borehole location.

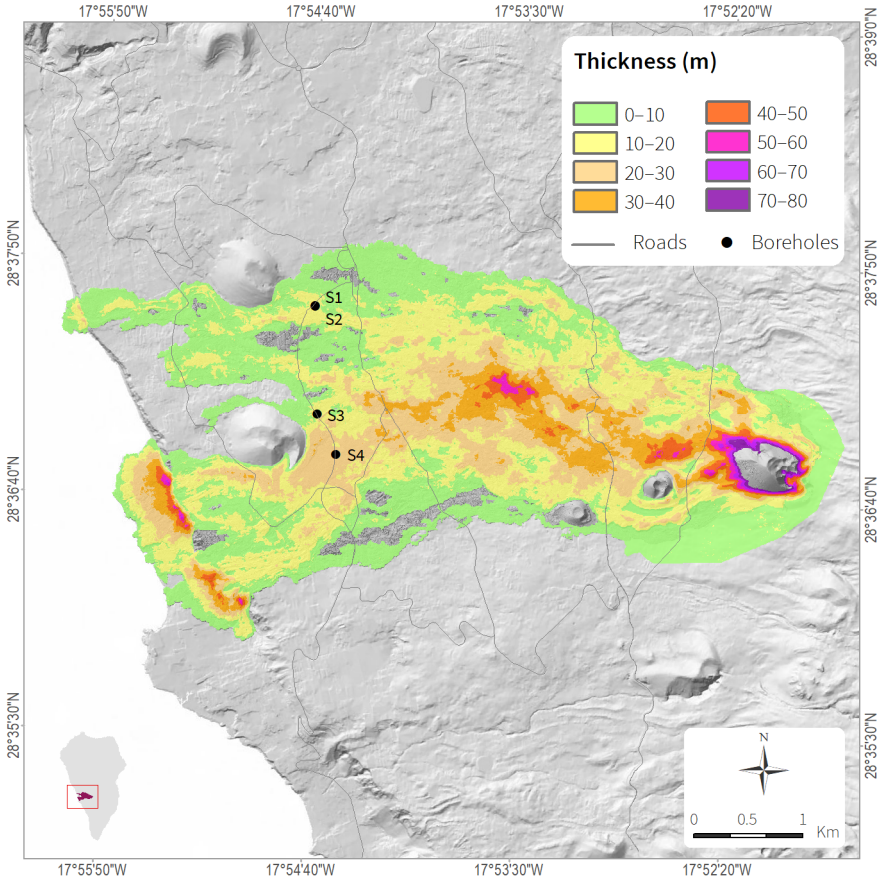

Figure 6. Thickness map of lava flows and borehole's location.

Figure 7. Borehole drilling in hot lavas, August 2022 (**left**), and Georadar survey to detect cavities, October 2022 (**right**).

3.2. Geophysical Investigations

Seismic investigations using spectral analysis of surface waves (SASW) have been conducted on the slopes of the volcanic cone to identify the composition and thickness of the materials, which consist of pyroclasts and lava flows. Figure 8 shows a geophysical profile of a slope formed by alternating layers of basaltic material, lapilli, and ashes. Additionally, electromagnetic methods employing ground-penetration radar techniques (Figure 7) have been applied to identify cavities and volcanic caves located beneath the ground surface. Figure 9 shows several electromagnetic anomalies originating from cavities. Details of the geophysical equipment used in the surveys are included in Appendix A.

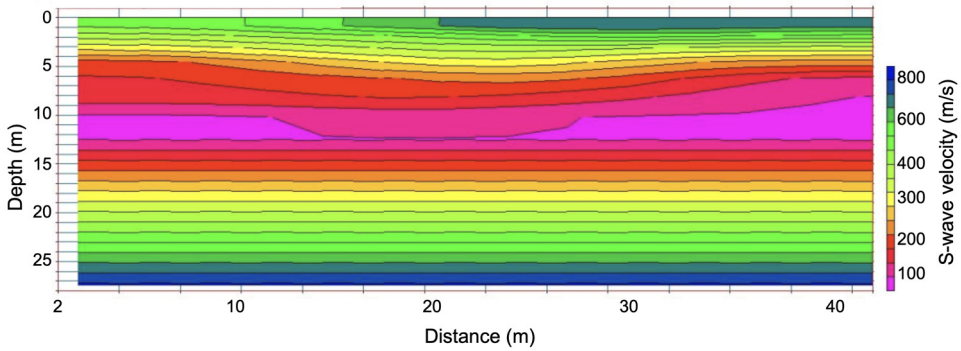

Figure 8. Geophysical cross section of the volcanic cone slope obtained through seismic spectral analysis of surface waves techniques (SASW).

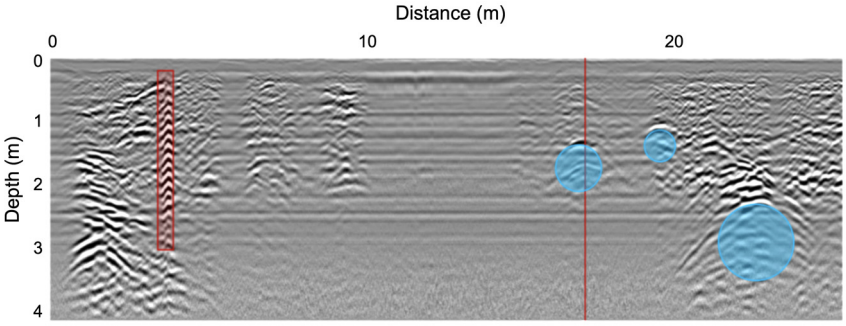

Figure 9. Lava flow section using ground-penetration radar techniques to identify cavities and volcanic caves in pahoehoe lavas, depicted in blue. The red color corresponds to materials with high electromagnetic conductivity.

3.3. Temperature Measurements

Surface temperatures were measured using both airborne thermographic cameras on drones and direct measurements on outcrops with a thermographic camera. The drone utilized was the DJI Matrice 300 RTK model, equipped with a DJI Zenmuse H20T thermal camera and a 24 mm wide-angle lens (display field of view DFOV: 82.9°) with 12 MP resolution, as well as a LiDAR system. Temperature measurements at different depths inside the boreholes were obtained using dataloggers. Temperature recording began on 2 August 2022 and continues to the present day. Figure 10 displays the temperatures recorded between 2 August 2022 and 4 July 2023.

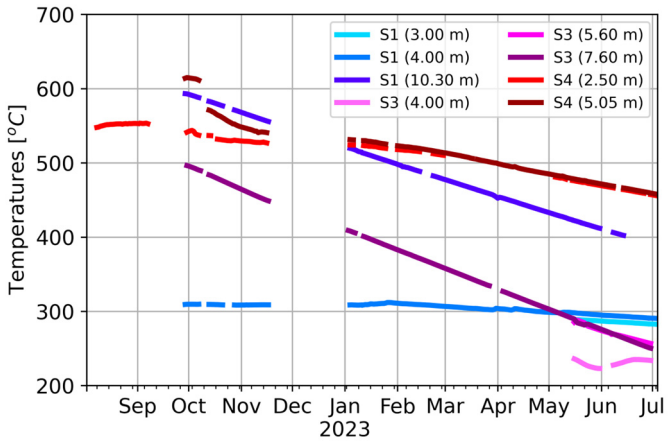

Figure 10. Temperatures measured inside the boreholes at different depths between 2 August 2022 and 4 July 2023.

Regarding the influence of climatic conditions on lava temperatures, it appears that climate does not have a significant impact in the case of La Palma on lava flow temperatures. La Palma, like the rest of the Canary Islands, has a Subtropical-Atlantic climate influenced by the ocean currents of the Gulf Stream and the North trade winds, with warm summers and cool, humid winters, and average annual temperatures of 21 °C. The climate on the western slope of the island, where the Tajogaite volcano and lava flows are located, is characterized by mild winters and warm summers. Annual distribution of precipitation occurs mainly during the winter months, averaging 89 mm, while the rest of the year experiences low precipitation. The average annual humidity is 76%, and the UV Index is 6. The trade winds provide a constant breeze, that not only cools the atmosphere but also helps regulate temperatures.

4. Cooling Rates of Lava Flows' Estimation

The cooling rates of lava flows have been estimated in certain volcanoes around the world, such as Mauna Loa and Kilauea in Hawaii [7,24], Okmok volcano in Alaska [10], Holuhraun volcano in Iceland [25], and Lonquima volcano in Chile [26]. However, these authors did not provide validation results or applicable methodologies for the La Palma eruption; consequently, we had to develop a new methodology based on in situ data and reconstruction requirements (Section 5).

4.1. Cooling Models

To estimate the cooling times of the lava flows, two cooling models have been developed: the homogeneous model and the heterogeneous model. In the first one, all the lavas are considered as a single medium composed of the same material and formed by isotropic and homogeneous basaltic lavas and, therefore, with consistent physicochemical properties, without considering the total thickness of the lava flow. On the other hand, the second model considers a heterogeneous and anisotropic medium, characterized by different types of lithologies, and it takes into account the various layers of lavas, their thickness, composition, and thermal conductivity, as well as the total thickness of the entire lava flow.

The homogeneous model assumes an isotropic material and does not account for variations in lava flow thickness, which limits its applicability to regions where the thickness is above approximately 15 m.

The heterogeneous model attempts to incorporate lithology and thermal properties, allowing us to include pahoehoe lavas. However, this model also has the same thickness limitation (it is less applicable in regions where the lava flow thickness is below approximately 15 m). Additionally, it requires detailed lithological data, necessitating boreholes for accurate application. As more borehole data become available in future studies, we anticipate that the model will better align with observed data.

The two cooling models, homogeneous and heterogeneous, are based on Newton's Cooling Law (1792), recently reviewed by Maruyama and Moriya [27], which defines the cooling coefficient (λ), which relates the time it takes for a body to cool from an initial temperature to a lower one. In our study area, an initial temperature of 1100 °C and a final temperature of 20 °C were considered, the latter corresponding to the average surface air temperature.

The cooling coefficient is expressed by the following differential equation, indicating the cooling rate of the body under consideration:

$$\frac{dT}{dt} = -\lambda(T - T_{amb}) \quad (1)$$

where T is the temperature of the body under analysis (variable), t is the time, and T_{amb} is the air temperature. The minus sign indicates the natural process of temperature decay that a body undergoes when it is at a higher temperature than the air temperature. The cooling coefficient is a constant parameter whose dimension is the inverse of time (s^{-1} in SI), i.e., synonymous with velocity, so that the cooling coefficient can be considered as a

cooling rate. If the air temperature is assumed to be constant, Expression (1) can be reduced to the following:

$$dT = -\lambda(T - T_{amb})dt \Rightarrow \frac{dT}{T - T_{amb}} = -\lambda dt \quad (2)$$

$$\int \frac{dT}{T - T_{amb}} = \int -\lambda dt = -\lambda \int dt \quad (3)$$

$$ln(T - T_{amb}) = -\lambda t + C \quad (4)$$

$$T - T_{amb} = e^{-\lambda t + C} = e^{-\lambda t} \cdot e^{C} = \tau \cdot e^{-\lambda t} \quad (5)$$

Equations (4) and (5) are equivalent, with Expression (5) being the one used to estimate the cooling coefficient. It must be taken into account that both C and τ are constants, so both values have been calculated applying an Initial Values Problem solution, in which the initial temperature is assumed to be known, i.e., when t = 0. Since in this case the exponential model has been applied, τ has been calculated by means of the following expression:

$$T(t = 0) = T(0) = T_0 \quad (6)$$

$$T_0 - T_{amb} = T \cdot e^{-\lambda \cdot 0} = \tau \quad (7)$$

$$T(t) = (T_0 - T_{amb}) \cdot e^{-\lambda t} + T_{amb} \quad (8)$$

where (8) is the equation defining the cooling coefficient. The initial cooling time of the lava flows has been taken as the time corresponding to the end of the eruption (23 December 2021).

4.2. Cooling Coefficients Estimated from Newton's Cooling Law

The time series of temperatures measured inside the boreholes during the period from 2 August 2022 to 4 July 2023 was used, and Expression (8) was applied to estimate the cooling coefficient, taking the temperature of 1100 °C corresponding to the initial cooling date, and 20 °C for the average air temperature in the study area. To measure the temperatures inside the boreholes, data loggers connected to probes installed at the following depths were used:

- 3.00, 4.00, and 10.30 m depths in borehole S1, and at 4.00, 5.60, and 7.60 m depths in borehole S3, both in aa lava flows.
- 2.50 m and 5.05 m depths in borehole S4 in pahoehoe lava flows. Borehole S2 has not been included due to erroneous temperature readings.

Given the oscillatory temperature regime observed in the surface layers of the boreholes due to the incidence of solar radiation, temperature data obtained at depths of less than 2.5 m have not been considered, nor have temperature data that could be altered by proximity to roads under construction [9].

Cooling coefficients have been obtained as a function of the data of each borehole and the depth of temperature measurement, by means of Least-squares Adjustment curves (Table 2).

Table 2. Cooling coefficients calculated from Newton's Law in the boreholes.

Borehole	Depth (m)	Cooling Coefficient (day^{-1})
S1	3.00	0.002631 ± 0.000008
	4.00	0.00314 ± 0.00004
	10.30	0.00201 ± 0.000006
S3	4.00	0.00307 ± 0.00002
	5.60	0.002747 ± 0.000001
	7.60	0.002742 ± 0.000004
S4	2.50	0.00207 ± 0.00004
	5.05	0.00183 ± 0.00001

4.3. Cooling Coefficients for Homogeneous Conditions

The homogeneous model assumes that the lava flows are of the aa type and consist solely of compact basalts with a continuous and uniform structure; it also assumes that their thermal and lithological properties are homogeneous and isotropic.

Based on the data obtained from boreholes S1 and S3 (Table 2), an exponential fit has been performed in order to estimate the temperatures at different depths. The result of the cooling coefficient obtained is as follows:

$$\lambda_{\text{homo}}(P) = (2.9 \pm 0.1)\cdot 10^{-3}\cdot e^{-(1\pm 10)\cdot 10^{-6}\,\cdot\, P^{6\pm 5}}(\text{days}^{-1}) \quad (9)$$

where λ_{homo} is the cooling coefficient under homogeneous conditions for aa lavas and P is the depth of temperature measurement. The range of validity of this expression is between 3 m and 10.3 m depths, inclusive. Figure 11 shows the obtained fitting curve as a function of the cooling coefficient.

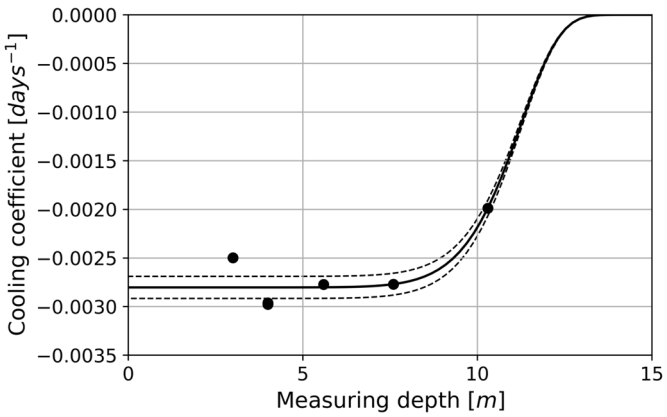

Figure 11. Fitting curve obtained from Expression (9) as a function of depth and cooling coefficient (Table 2) in aa lava flows for homogeneous conditions. The dashed lines indicate the margin of error.

From Expression (9), the cooling times necessary to reach certain depths of 3, 5, 7, and 10 m (Table 3) have been estimated. The resulting cooling curves are shown in Figure 11. As can be seen, the lower the cooling coefficient, the longer the cooling times, or the greater the depths.

Table 3. Cooling coefficients as a function of depth, temperature, and cooling times for homogeneous conditions.

Depth (m) (*)	λ ($days^{-1}$)	Cooling Time (Days)		
		400 °C	100 °C	50 °C
3	0.00295	354	882	1214
5	0.00292	357	891	1226
7	0.00279	374	932	1283
10	0.00212	492	1227	1690

(*) Depth of temperature measurement. λ: cooling coefficient. Cooling days counted from the start of cooling (23 December 2021).

Figure 12 shows the simulated curves for different depths using the homogeneous model. As expected, the greater the depth, the longer the cooling time. However, for depths between 3 and 7 m, the differences are hardly noticeable, as can be seen by comparing this last graph with the data collected in Figure 11 and Table 3.

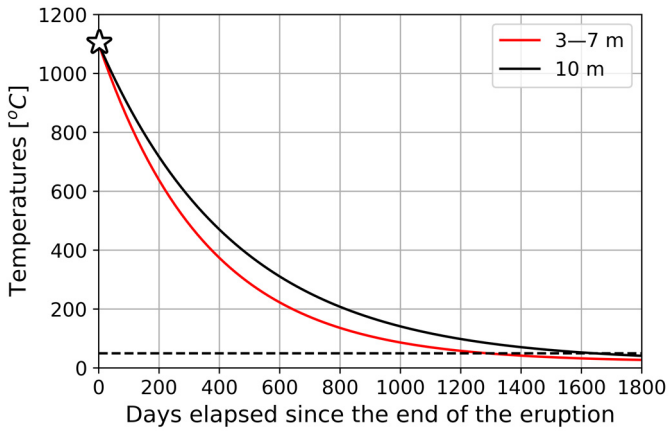

Figure 12. Cooling curves under homogeneous conditions as a function of depth in aa lava flows. ☆: initial cooling temperature. The dashed line marks a temperature of 50 °C.

4.4. Cooling Coefficients for Heterogeneous Conditions

The heterogeneous model considers the specific geological characteristics of several sites where boreholes have been drilled and temperatures have been measured at different depths, down to 10 m. The thickness of each lava layer, its lithology, and petrological composition were determined. The total thickness of the lava flows was estimated using GIS tools by comparing digital terrain models from before and after the 2021 eruption (see Figure 6). The thermal conductivities of each material were estimated by averaging the thermal conductivity values of materials with the same petrological composition as Canary Island lavas (Table 4). The cooling coefficients obtained previously from Newton's Cooling Law (Table 2) were used, and each type of lithology composing the lava flows was differentiated: olivine–pyroxene basalts and lava scoria, as well as the presence of cavities, in which case the air conductivity was considered. In the heterogeneous model, both aa and pahoehoe lava flows have been analyzed.

Table 4. Average thermal conductivities of materials [28].

Material	Thermal Conductivity ($Wm^{-1}K^{-1}$)
Basalt	3.7 ± 0.3
Scoria	1.85 ± 0.25
Air (cavity)	0.02

The depths at which the temperatures were measured in the boreholes were the same as those in the homogeneous model:

- aa lava flows: S1 at 3.00, 4.00, and 10.30 m depths; and S3 at 4.00, 5.60, and 7.60 m depths.
- pahoehoe lava flows: S4 at 2.50 and 5.05 m depths.

On the other hand, to obtain the cooling coefficient under heterogeneous conditions, three new parameters have been defined:

1. Thermal Conductivity Reduction Coefficient (CRC), that takes into account the thermal conductivity of each material (κ) and its thickness, as follows:

$$CRC = \frac{\kappa_S}{\kappa_b} \tag{10}$$

$$\Delta CRC = \frac{\Delta\kappa_S}{\kappa_b} + \frac{\kappa_S}{{\kappa_b}^2}\cdot\Delta\kappa_b = \frac{\Delta\kappa_S}{\kappa_b} + \frac{CRC}{\kappa_b}\cdot\Delta\kappa_b \tag{11}$$

where κ_s is the thermal conductivity of the materials above a certain depth at which the temperature has been measured, and κ_b is the thermal conductivity of the basalt. κ_s can be estimated according to the following polynomial expression:

$$\kappa_S = x_b\cdot\kappa_b + x_e\cdot\kappa_e + x_a\cdot\kappa_a \tag{12}$$

$$\Delta\kappa_S = x_b \cdot \Delta\kappa_b + x_e \cdot \Delta\kappa_e + x_a \cdot \Delta\kappa_a \quad (13)$$

where x_n represents the ratio, or nth fraction, of a given material to the borehole length, and varies between 0 and 1, and κ_n represents the nth thermal conductivity of that material, where n can be *b* (basalt), *e* (scoria), and *a* (cavity).

2. Thickness Ratio (TR), which relates the depth of temperature measurement and the total thickness of the whole lava flow, as both parameters are related to the process and cooling times. TR can be expressed as:

$$\mathrm{TR} = \frac{\mathrm{z}}{\mathrm{E}} \quad (14)$$

where z is the measuring depth, and E is the thickness of the lava flow at that point.

3. Cooling Factor (CF), which relates the CRC to the TR, and is expressed as follows:

$$\mathrm{CF} = \mathrm{CRC}^{\mathrm{n}} \cdot (1 - \mathrm{a} \cdot \mathrm{TR}) \quad (15)$$

$$\Delta\mathrm{CF} = \left[\mathrm{CF} \cdot \log(\mathrm{CRC}) \cdot \Delta\mathrm{n} + \mathrm{n} \cdot \frac{\Delta\mathrm{CRC}}{\mathrm{CRC}}\right] \cdot (1 - \mathrm{a} \cdot \mathrm{TR}) + \frac{\Delta\mathrm{a}}{1 - \mathrm{a} \cdot \mathrm{TR}} \quad (16)$$

where a and n are known parameters and Δa and Δn are their corresponding errors, respectively, the calculation of which is shown in Appendix B. The results obtained are as follows:

$$\mathrm{a} = 0.55 \pm 0.01$$

$$\mathrm{n} = 0.32 \pm 0.01$$

Applying these results to Expressions (15) and (16), we obtain:

$$\mathrm{CF} = \mathrm{CRC}^{0.32 \pm 0.01} \cdot [1 - (0.55 \pm 0.01) \cdot \mathrm{TR}] \quad (17)$$

$$\Delta\mathrm{CF} = \left[\mathrm{CF} \cdot \log(\mathrm{CRC}) \cdot 0.01 + 0.32 \cdot \frac{\Delta\mathrm{CRC}}{\mathrm{CRC}}\right] \cdot (1 - 0.55 \cdot \mathrm{TR}) + \frac{0.01}{1 - 0.55 \cdot \mathrm{TR}} \quad (18)$$

Table 4 shows the average thermal conductivity values for the olivine–pyroxene basalts and slags, as well as the assumed theoretical value for the thermal conductivity of air. Table 5 shows the thickness data for each material and their relative proportion with respect to the borehole length.

Table 5. Thicknesses of materials and their relative proportion to the borehole length.

Borehole	Lithology	Thickness (m) (*)	Ratio (xn)
S1	Basalt	2.60	0.25
	Scoria	1.40 + 6.30 = 7.70	0.75
	Air	0.00	0.00
S2	Basalt	1.40	0.56
	Scoria	1.10	0.44
	Air	0.00	0.00
S3	Basalt	1.70 + 2.00 = 3.70	0.49
	Scoria	0.50 + 3.40 = 3.90	0.51
	Air	0.00	0.00
S4	Basalt	0.80	0.16
	Scoria	2.05	0.40
	Air	2.20	0.44

(*) Total thickness of the lava flow.

From the thermal conductivity and thickness data (Tables 3 and 4), Expressions (10)–(13) have been applied to obtain the thermal Conductivity Reduction Coefficient (CRC) as a function of depth (Table 6).

Table 6. Thermal Conductivity Reduction Coefficient (CRC) as a function of depth.

Borehole	Depth (m) (*)	CRC
S1	3.00	0.77 ± 0.13
	4.00	0.83 ± 0.15
	10.30	0.63 ± 0.12
S3	4.00	0.71 ± 0.13
	5.60	0.65 ± 0.12
	7.60	0.75 ± 0.13
S4	2.50	0.32 ± 0.10
	5.05	0.36 ± 0.10

(*) Depth of temperature measurement.

From Expression (14), the Thickness Ratios shown in Table 7 have been estimated.

Table 7. Thickness Ratio (TR) at different depths.

Borehole	Thickness (m)	Depth (m)	TR
S1	11.99	3.0	0.25
		4.0	0.33
		10.30	0.86
S3	13.23	4.0	0.30
		5.60	0.42
		7.60	0.57
S4	19.44	2.50	0.1
		5.05	0.26

Both CRC and TR are dimensionless and vary between 0 and 1. Thus, CRC = 0 would mean void, and a value of CRC = 1 would indicate that the borehole column would be entirely made up of basalt. A value of TR = 0 would mean a depth of 0 (surface), while a value of TR = 1 would correspond to a measurement depth equivalent to the total thickness of the lava flow at that point.

Table 8 shows the results obtained by applying Expressions (17) and (18) to the estimation of the Cooling Factor (CF). These results indicate that the higher the cooling factor (CF), the higher the cooling rate of the lava flows, and it varies between 0 and 1, as in the previous CRC and TR parameters. On the other hand, the higher the CRC, the higher the cooling rate, while the higher the TR, the lower the cooling rate.

Table 8. Cooling Factors (CF) as a function of depth.

Borehole	Depth (m)	CF
S1	3.0	0.79 ± 0.05
	4.0	0.77 ± 0.05
	10.3	0.46 ± 0.03
S3	4.0	0.74 ± 0.05
	5.6	0.66 ± 0.04
	7.6	0.63 ± 0.04
S4	2.5	0.61 ± 0.07
	5.05	0.59 ± 0.06

From the CF values estimated for heterogeneous conditions (Table 8), and the cooling coefficients calculated from Newton's Cooling Law (Table 2), the cooling coefficient for heterogeneous conditions has been obtained, using the following expression:

$$\lambda_{\text{hetero}} = -(3.7 \pm 0.5) \cdot 10^{-3} \cdot \text{CF} - (0.5 \pm 3.3) \cdot 10^{-4} \quad (19)$$

where λ_{hetero} is the estimated cooling coefficient for heterogeneous conditions.

Figure 13 shows the relationship between the cooling coefficient estimated from Newton's Cooling Law and the Cooling Factor (CF), obtaining a correlation coefficient (R) of 0.9797.

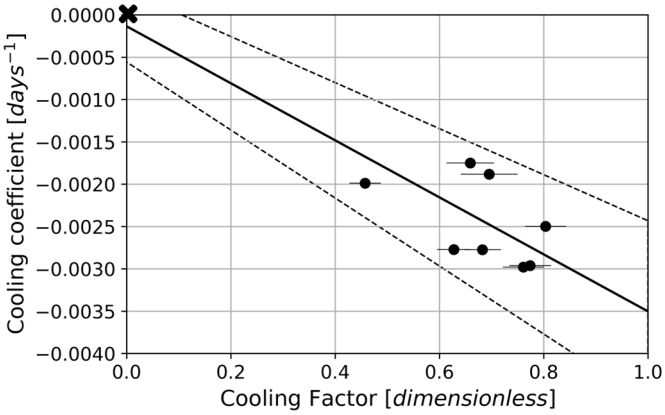

Figure 13. Fit curve obtained from Expression (19), as a function of the cooling factor and cooling coefficient (Table 2) for heterogeneous conditions. The dashed lines indicate the margin of error. **X**: theoretical data.

These results indicate that the higher the cooling coefficient, the higher the cooling rate should be, which is compatible with Expression (19) and with the results shown in Figure 13. The point X shown in Figure 13 represents a theoretical value corresponding to a cooling factor equal to zero, according to Expression (17).

Tables 8 and 9 show the cooling times to reach certain temperatures as a function of depth and the cooling coefficients obtained according to the heterogeneous model.

Table 9. Cooling times required to reach certain temperatures as a function of cooling coefficients and depth, according to the heterogeneous cooling model, for aa lava flows (borehole S1).

P (m)	λ (Days^{-1})	CRC	TR	CF	Cooling Time (Days) (*)		
					400 °C	100 °C	50 °C
3	0.00300	0.77	0.25	0.79	348	868	1195
5	0.00268	0.76	0.42	0.71	390	972	1338
7	0.00230	0.69	0.58	0.60	455	1133	1560
10	0.00180	0.63	0.83	0.47	582	1449	1995

P: Temperature measurement depth. λ: Cooling coefficient according to the heterogeneous model. CRC: Thermal conductivity reduction coefficient. TR: Thickness ratio. CF: Cooling factor. (*) Cooling days counted from the start of cooling (23 December 2021).

From the data shown in Tables 8 and 9, a series of cooling curves have been fitted (Figures 14 and 15), the first one corresponding to the data in Table 9, and the second one to Table 10, corresponding to aa lava flows, within a time interval of 1800 days from when the lava flow began to cool.

The cooling curves, obtained from data from boreholes S1 and S3, located 990 m apart, show similar trends, but with some differences due to variations in thickness and thermal conductivity that reflect variable and heterogeneous behavior.

Figures 14 and 15 show the cooling curves simulated from the heterogeneous model for boreholes S1 and S3, respectively. In both cases, it can be clearly seen that the deeper the borehole, the lower the cooling rate, i.e., the longer it takes to reach a certain temperature. The differences between the two boreholes are miniscule; but it can be seen, for example, that for a depth of 10 m, the cooling process is faster for borehole S3 than for S1. This is because the proportion of scoria in the first is lower than in the second, as the thermal conductivity of the scoria is lower than that of the basalt.

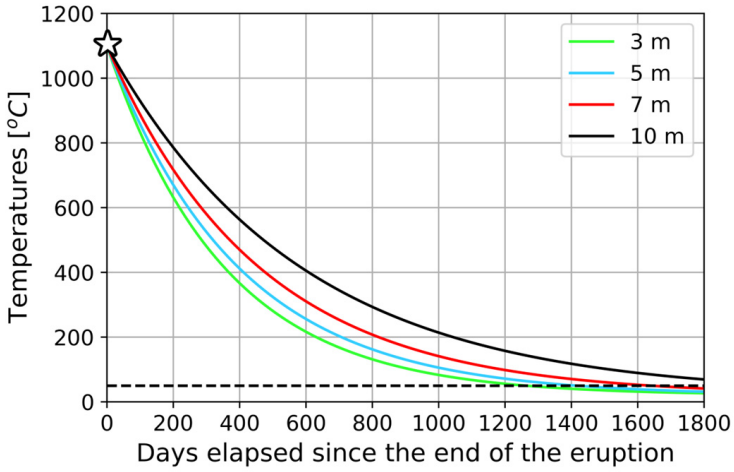

Figure 14. Cooling curves at different depths for heterogeneous conditions in aa lava flows, borehole S1. ☆: initial cooling temperature. The dashed line marks a temperature of 50 °C.

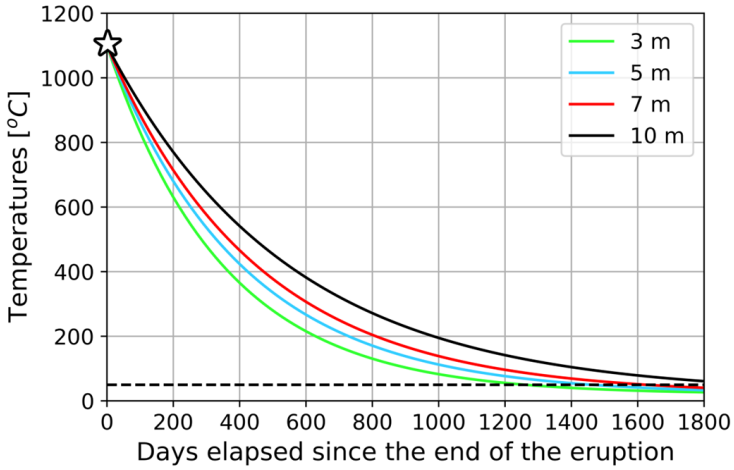

Figure 15. Cooling curves at different depths for heterogeneous conditions in aa lava flows, borehole S3. ☆: initial cooling temperature. The dashed line marks a temperature of 50 °C.

Table 10. Cooling times required to reach certain temperatures as a function of cooling coefficients and depth, according to the heterogeneous cooling model, for aa lava flows (borehole S3).

P (m)	λ (Days^{-1})	CRC	TR	CF	Cooling Time (Days) (*)		
					400 °C	100 °C	50 °C
3	0.00301	0.78	0.25	0.80	347	864	1190
5	0.00257	0.67	0.42	0.68	406	1012	1393
7	0.00233	0.72	0.58	0.61	449	1118	1539
10	0.00194	0.81	0.83	0.51	537	1339	1844

P: Temperature measurement depth. λ: Cooling coefficient according to the heterogeneous model. CRC: Thermal conductivity reduction coefficient. TR: Thickness ratio. CF: Cooling factor. (*) Days counted from the start of cooling (23 December 2021).

Figure 16 summarizes the main methodological steps to be followed for the calculation of the cooling coefficients for homogeneous and heterogeneous conditions.

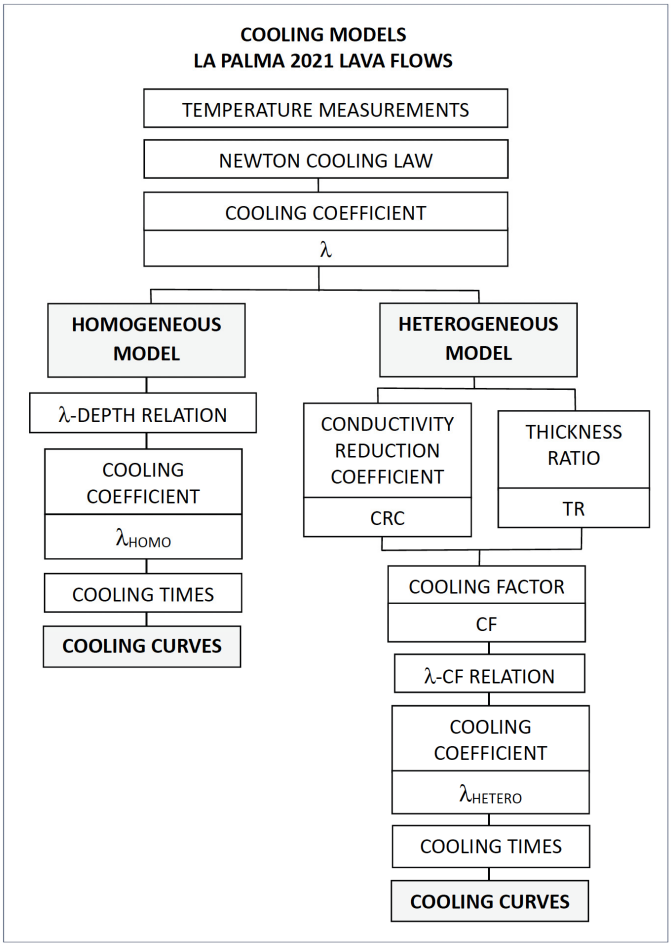

Figure 16. Cooling coefficients and cooling curves calculation flowchart.

4.5. Comparative Analysis between Temperatures Measured In Situ and Those Estimated by Cooling Models

To compare the temperature differences between the instrumentally recorded values and those estimated by the cooling models, boreholes S1 and S3 have been selected due to their smaller dispersions of results compared to the other boreholes; these boreholes were used to compare the two models and estimate the deviations with respect to the recorded temperatures. The results are presented in Table 11.

Table 11. Differences between instrumentally measured temperatures and those estimated according to the homogeneous model (aa lava flows).

Borehole	Depth (m) [1]	Sign [2]	Deviation (%) [3]
S1	3	−	12.81
	4	+	10.98
	10.3	+	1.82
S3	4	+	5.37
	5	−	6.26
	7	+	1.30

(1) Depth of temperature measurement. (2) Positive sign indicates higher estimated temperature than measured (overestimation), and negative sign indicates lower estimated temperature than measured (underestimation). (3) Percentage deviation from measured values.

The results shown in Table 11 indicate that in the homogeneous model, the maximum deviation was 12.81%, with values of less than 6% predominating, while for the heterogeneous model, in Table 12, the highest value was 16.34%, with deviations of less than 11%.

In both models, the overestimation of temperatures predominates, which is equivalent to longer cooling times, this difference not being significant given the low deviation of temperatures between the two estimated models and the instrumental measurements.

Table 12. Differences between instrumentally measured temperatures and those estimated according to the heterogeneous model (aa and pahoehoe lava flows).

Borehole	Depth (m) [1]	Sign [2]	Deviation (%) [3]	Lava Flow Type
S1	3	−	16.34	aa
	4	+	10.91	
	10.3	+	10.66	
S3	4	+	10.91	aa
	5	+	10.83	
	7	+	15.70	
S4	2.5	−	10.89	pahoehoe
	5.05	−	13.97	

(1) Depth of temperature measurement. (2) Positive sign indicates higher estimated temperature than measured (overestimation), and negative sign indicates lower estimated temperature than measured (underestimation). (3) Percentage deviation from measured values.

5. Applications to Territorial Reconstruction and Georisk Mitigation

5.1. Thermal Behavior of Lava Flows Applied to Infrastructure Reconstruction

The thermal behavior of lava flows is characterized by their lithological composition and thermal properties, as described in Sections 2 and 4, respectively. Essentially, lava flows consist of a sequence of scoriaceous breccias and compact basaltic layers, with an upper crust of breccias of low thermal conductivity and a rapid cooling rate, in direct contact with the surface temperature; and an inner basaltic core of high thermal conductivity and a very slow cooling rate. As a result, the upper crust functions as an effective heat insulator relative to the basaltic inner core.

Thirty experimental in situ tests were conducted along a newly built road crossing lava flows from the La Palma 2021 eruption, and temperatures were measured at 15 cm and 40 cm depths at a distance from the roadside of between 4 m and 20 m. The scoriaceous upper crust had been excavated in those sites located near the roadside, presenting much higher temperatures than the sites located farther away from the roadside, where the upper crust had not been excavated. The results have shown that 60% of the temperature values exceeded 30 °C in the sites located near the road, while in the sites farther away from the road, 87% of temperatures were equal to or below 30 °C. Table 13 and Figure 17 summarize these results.

Table 13. Temperature ranges of lava flows and distances to the road sides.

Near the Roadside		Away from the Roadside	
T °C	% Measurements	T °C	% Measurements
≤30°	87	≤30°	40
31°–100°	6	31°–100°	26
>100°	7	>100°	34

The highest temperatures have been measured at a distance from the roadside of less than 8 m (Table 13; Figure 17), while the lowest temperatures have been measured more than 15 m from the roadside (Figure 18). Extensive excavation of the lava flows was carried out during road construction, and most of the first few meters of lava, including the upper crust, was removed.

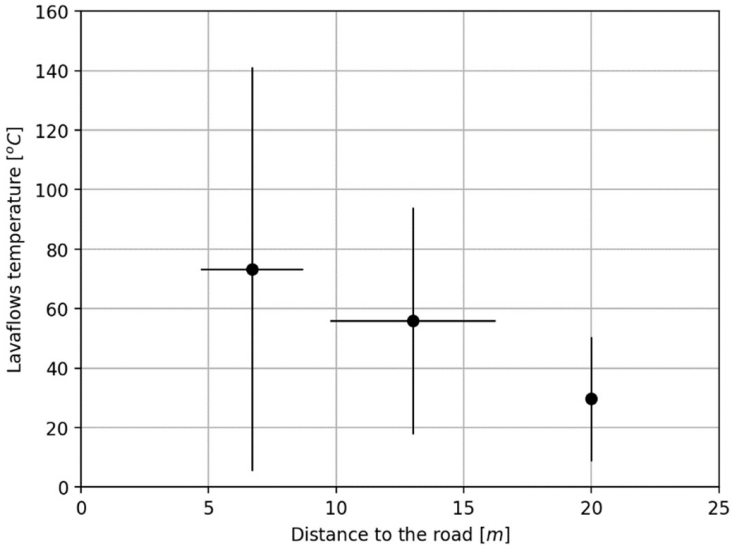

Figure 17. Mean values of lava flows temperatures obtained 2 years after the volcanic eruption at different distances from the roadsides.

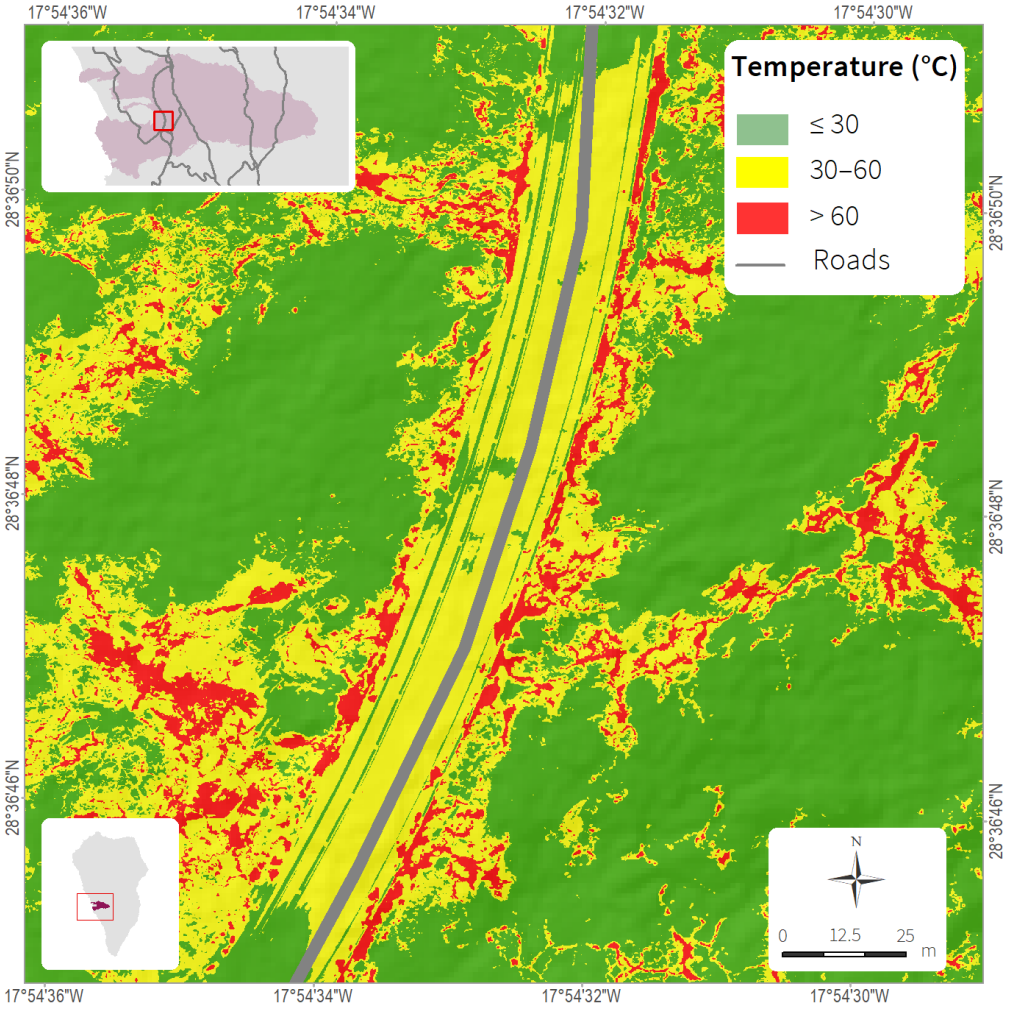

Figure 18. Map of surface lava flow temperatures measured in situ by drones in the vicinity of a new road built two years after the eruption. The area is dominated by pahoehoe-type lava flows.

5.2. Thermal and Geological Conditioning Factors

The infrastructure reconstruction projects have been impacted by the need to start work as soon as possible under extreme geological conditions due to the high temperatures of the lava flows and the long cooling times, which made short- or medium-term reconstruction practically unfeasible. Under these thermal and geological constraints, possible solutions were studied based on experiences in other regions and, mainly, on the development of new alternatives.

Using the lava flows' cooling models, cooling times to reach temperatures compatible with the type of activity being carried out were estimated. For this purpose, thermal, geological, and geotechnical investigations, summarized in Figure 19, have been conducted, applied to each of the reconstruction activities described below.

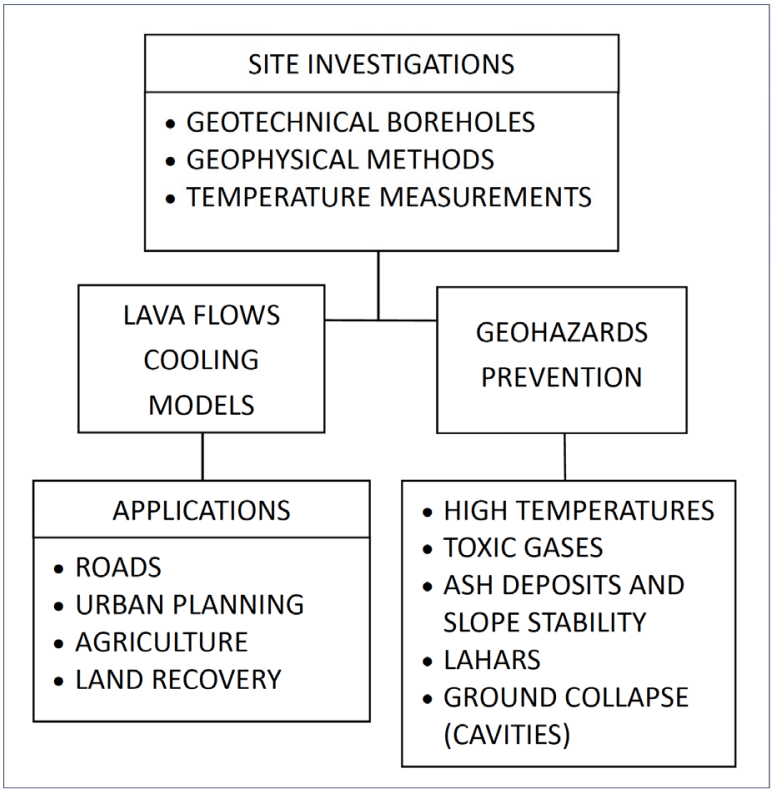

Figure 19. Thermal and geomechanical investigations applied to the reconstruction and territorial recovery of La Palma.

5.3. Agriculture Recovery Applications

One of the main economic resources of the island of La Palma comes from agriculture, particularly banana cultivation. The lava flows from the 2021 eruption destroyed over 7 km^2 of crops in the most productive area [18]. In 2023, thermal and geotechnical investigations were initiated for the agricultural recovery of the areas devastated by the lava. These investigations involved temperature measurements through drone flights.

The results of surface temperature measurements have been mostly below 30 °C; however, several areas with higher values have been identified, often ranging between 60 °C and 100 °C, attributed to thermal anomalies. These anomalies are more frequent in pahoehoe-type lava flows than in aa-type flows. Figure 20 represents a quadratic fit to the data according to the type of lava flow and its thickness, with higher temperatures observed for thicker lava flows.

Figure 21 shows 4 maps summarizing the results of the investigations conducted in the so-called agricultural recovery zone: lava thickness map (A); surface temperatures map of the lava flows in 2023 (B); and temperature suitability maps for agricultural applications in 2024 (C) and 2025 (D), based on lava flow cooling models. In the latter cases, suitability conditions have been assumed for lava flows surface with temperatures equal to or less than 30 °C as a threshold value, being determined by the maximum acceptable temperature of the roots of the banana plant. Unsuitable conditions have been identified in some areas with temperatures above 60 °C (red spots), attributed to thermal anomalies. There are many reasons for non-homogeneous localized "hot spots" on the surfaces of cooling flows, although only for flows of greater thickness (more than two meters), since thin flows almost all cool pretty uniformly. On thicker flows, persistently warmer areas are all related to internal features. These can include irregular pre-eruption terrain, where the flows are much thicker in certain areas, to variations in texture (less dense "shelly" or fragmental lava retain less heat than dense concentrations in well-crystallized zones). Some persistently warm areas are associated with highly fractured or permeable zones, where heated volatiles can bring heat from adjoining zones to the surface (commonly marked by ephemeral subliminate deposits). Where subsurface pyroducts were long active, much heat can be concentrated in denser wall rocks, and can be areas of increased surface heating (usually found in linear or curved points above unseen (and commonly filled) pyroducts.

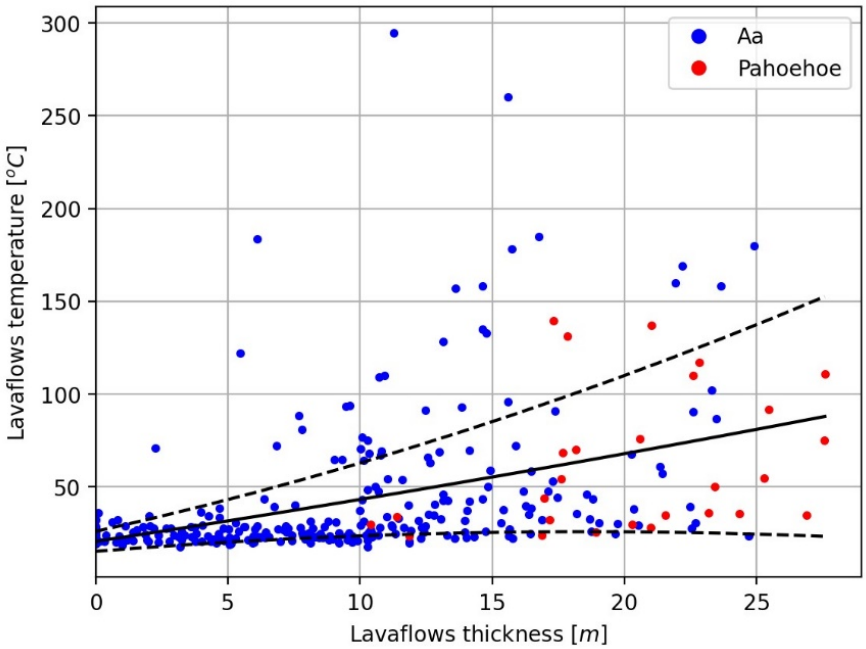

Figure 20. Temperature distribution as a function of the thickness of aa and pahoehoe lava flows. The solid line represents a quadratic adjustment of the data, illustrating the overall trend. The dashed lines indicate the error margins, providing a visual representation of the uncertainty in the data fitting.

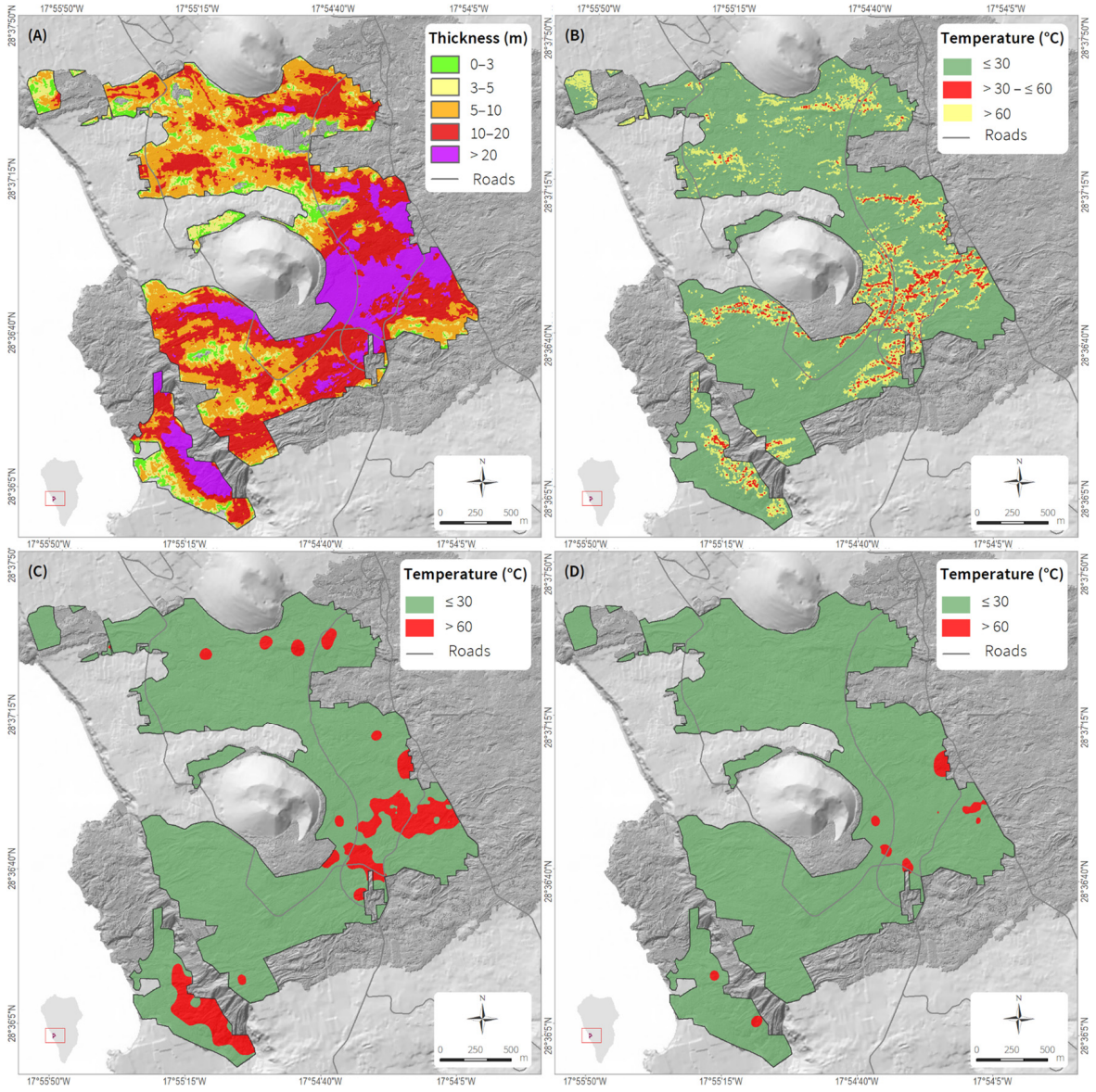

Figure 21. (**A**) Thickness map of lava flows for agricultural recovery purposes. (**B**) Map of surface temperature measured during 2023. (**C**,**D**). Maps of surface temperature estimated for 2024 and 2025 respectively according to cooling rate estimations.

Engineering Solution Based on Lava Flow Thermal Behavior

Given the need to recover agricultural activity in the shortest possible time, a potential solution has been developed to avoid the transmission of high temperatures to plant roots. For this purpose, a physical model based on Fourier's Law, also known as the heat equation, has been developed, which relates the spatial–temporal change in temperatures with the thermal conductivity of a material. The thickness required for a fill material composed of soil with low thermal diffusivity, acting as insulation material, has been calculated. This thickness aims to ensure that at a depth of 0.5 m, corresponding to the root depth of banana plants, the temperature remains below 30 °C, thereby safeguarding the roots from being affected by high temperatures.

It has been assumed that both the ambient air and the fill material have an initial temperature of 20 °C, and that the critical temperature the roots can withstand is 30 °C. Taking these assumptions into account, it was estimated that the earth fill thickness should be 2 m, the plant roots being at a depth of 0,5 m, for a lava flow temperature of 60 °C.

A safety factor of 2.0 has been considered in these calculations to account for possible uncertainties, thus obtaining a temperature of 33 °C at 0.5 m depth.

Table 14 shows an example of relationships between the surface temperature of the lava flow and the fill thicknesses required to achieve a temperature of 30 °C at a depth of 0.50 m, similar to that reached by plant roots as well as the temperatures that would be reached at 0.50 m depth if the fill thickness is 1.5 m. Thus, for a lava flow surface temperature of 50 °C and a 1.5 m thick soil fill, a temperature of 30 °C is obtained at the plant roots depth.

Table 14. Relationships between temperatures at the surface of lava flows and earth fill thicknesses required to reach temperatures compatible with plant root development at 0.5 m depth.

Lava Flow Surface Temperature (°C)	Fill Thickness (m) to Achieve a Temperature of 30 °C at 0.5 m Depth (Roots Depth)	Temperature (°C) at a Depth of 0.5 m (Roots Depth) for a Fill Thickness of 1.5 m
50	1.5	30
60	2.0	33
75	2.8	38
100	4.0	47
150	6.5	63
200	9.0	80
300	14.0	113

Based on the temperature data and the geotechnical conditions of the lava flows, the following thermal and geotechnical feasibility criteria have been proposed for the agricultural reclamation of the banana cultivation:

- A threshold value of 30 °C above which plant roots may be damaged has been proposed.
- In the case of surface temperatures above 30 °C and below 60 °C, it is recommended to build a 1.5 to 2 m thick low-thermal-conductivity earth fill, placed on top of the lava flows.
- For temperatures above 60 °C, it is necessary to wait for the lava flow to cool down to temperatures below 60 °C.

These criteria assume no excavation of the scoriaceous surface crust.

5.4. Road Construction on Hot Lava Flows

Several months after the eruption, lava flow temperatures exceeded 500 °C in numerous areas, both on the surface and at depths of a few meters, making it impossible to start road construction works in the short or medium term. Consequently, a solution based on the thermal behavior of the lava flows (Section 5.1) was proposed, summarized as avoiding excavation of the upper scoriaceous crust and constructing the road on top of the lava flows. This would require significant rockfills sourced from basaltic materials but would allow construction to begin on lava flows as early as 6 months to 1 year after the eruption, depending on the surface temperatures of the lavas and cooling times (Section 4). This type of solution would be advisable for low-cost roads, with its main advantage being the short time required to initiate the works and its lower complexity in execution.

Road construction was able to begin within 6 months after the eruption, and the experiences gained during construction have confirmed the viability of the proposed solution. Figure 22 shows two roads under construction. On the left, where no excavations were carried out, low temperatures were observed, while on the right photo excavations were carried out, resulting in high temperatures and gas emission. These same findings can be observed in Figures 17 and 18.

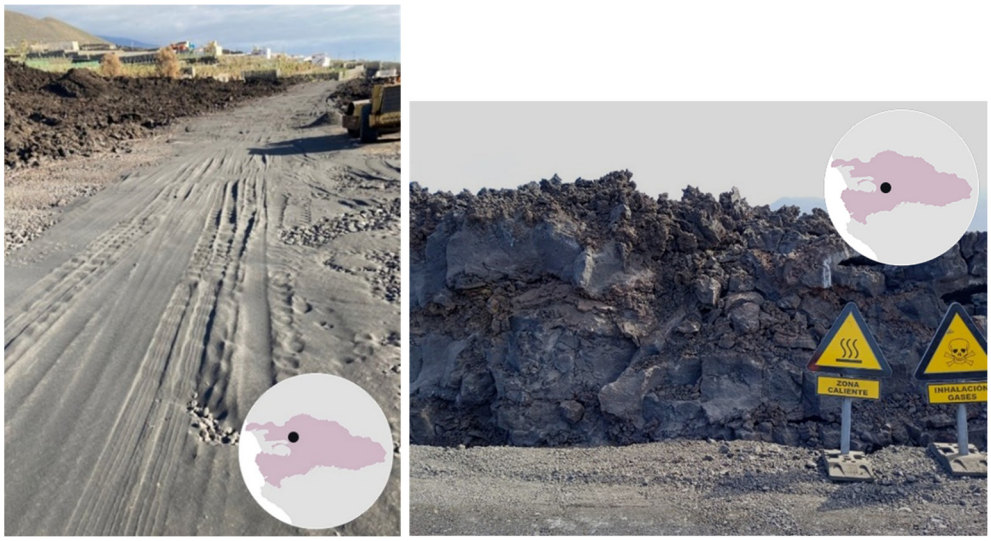

Figure 22. Road construction on hot lava flows 6 months after volcanic eruption of La Palma 2021, according to the proposed solution (**left**). Road excavation of lava flows and related hazard warning signs for high temperatures and gases at a site where the proposed solution was not implemented (**right**). The black points inside the circle indicate the sites where the photos were taken on the lava field (see Figure 3).

5.5. Urban Planning

The proposed land and urban planning projects have included three possible areas designated for new urban settlements located on lava flows, where thermal and geotechnical investigations were conducted to estimate the viability of these settlements for urban use, following the described methodologies (Figures 16 and 19).

Temperatures measured on the surface of the lava flows exceeded 50 °C in November 2022, and the cooling times required to reach temperatures at or below 30 °C, as a threshold value compatible with urban activities, were estimated from 3 years after the eruption, i.e., after 2024.

Figure 23 shows an example of the application of cooling rate lava flow models to urban planning purposes. Cooling times, temperatures, and depths have been considered according to land use requirements.

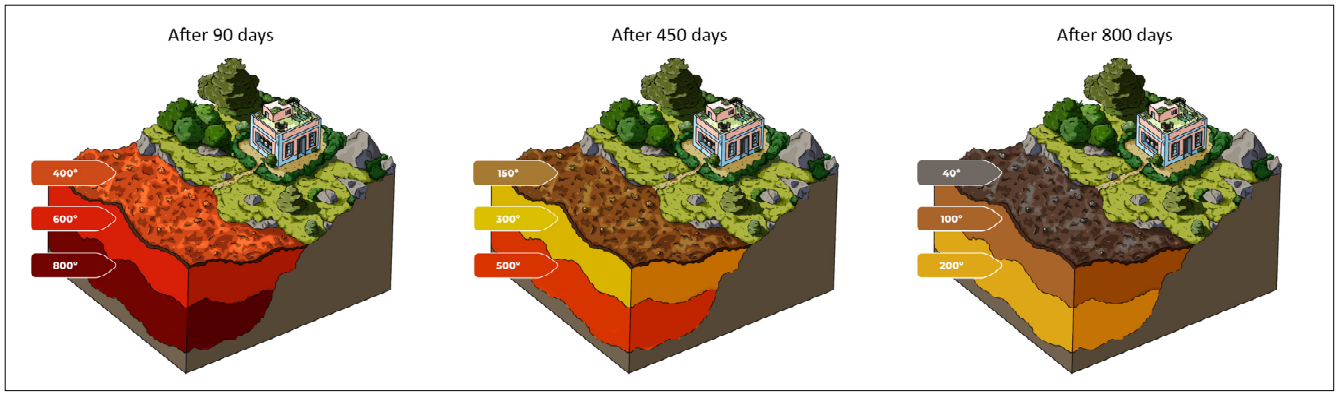

Figure 23. Cooling processes of the lava flows.

The thermal and geotechnical feasibility criteria recommended for urban planning were as follows:

- To start construction activities from 2025 onwards.
- The maximum temperature on the lava flow surface compatible with construction activities has been set at 30 °C, or the ambient temperature.

- Absence of volcanic cavities in the subsurface where infrastructures are supported must be ensured.
- Areas located on aa lava flows with a thickness not exceeding 10 m are favorable zones.
- Avoid construction on pahoehoe lava flows given their unfavorable thermal and geotechnical behavior, with frequent thermal anomalies due to high temperatures and the more frequent presence of cavities.
- Building height limited to one floor, avoiding basement excavation.

5.6. Georisk Prevention and Mitigation Measures

The following geological hazards have emerged after the volcanic eruption of La Palma 2021:

- High temperatures above the lava flows restrict any type of construction activity, particularly on thick lava flow deposits, for over five years.
- Toxic gases have affected two urban centers, forcing the evacuation of a part of their inhabitants.
- Accumulation of ash deposits with thicknesses of several meters have covered numerous houses, causing damage to urban areas, roads, infrastructure, and agricultural land.
- Lahars hazards associated with very intense rainfall in areas of ash deposits.
- Instability of the slopes of the new volcanic cone in the event of very intense rainfall.
- Ground collapses due to the sinking of cavities and lava tubes in the event of structural overloads or natural causes.

5.6.1. High Temperature Hazards of Lava Flows

At the end of the eruption, the temperature of the lava flows was 1100 °C, after which they began to cool. The time required to reach temperatures below 50 °C for approximately 10 m thick lava flows, according to the cooling rates, could exceed 4 to 5 years, depending also on factors other than thickness as previously discussed. These factors will have to be considered for future reconstruction projects. The proposed constructive solutions (Sections 5.3–5.5) would significantly mitigate the effects and consequences of high temperatures by allowing reconstruction and recovery works to commence in shorter time frames.

5.6.2. Toxic Gases Hazards

After the volcanic eruption in December 2021, some urban areas not directly damaged by lava flows were affected by high carbon dioxide (CO_2) emissions from the subsoil (CO_2 is a toxic gas at high concentration, as well as an asphyxiant gas, and may be lethal when present in concentrations higher than 15% volume). This situation forced the evacuation of a large part of the population of Puerto Naos and La Bombilla villages, located few km away from the lava flows. The base of the small cliff where La Bombilla is located, as well as the basements and garages of numerous buildings in Puerto Naos (Figure 24, right), seems to represent leaking pathways along which CO_2 gases associated with volcanic–hydrothermal activity rising to the surface. The CO_2 Alert Project (2024) aims to deploy a network of 1200 sensors of CO_2 concentration in these two urban areas, which represents a unique milestone, both for its scope and for its significance in monitoring the hazards associated with high CO_2 concentrations in inhabited areas. Beyond comprehending the complexities of gas dynamics, this project endeavors to deliver an effective solution, ensuring the safety of residents.

Figure 24. Measuring gases in a basement located in Puerto Naos, La Palma (**left**). Accumulated ash deposit near the volcanic cone (**right**).

5.6.3. Hazards from Instability of Volcanic Cone Slopes and Lahars

The stability conditions of the newly formed volcanic edifice of Tajogaite were analyzed to assess potential hazards. This edifice consists predominantly of pyroclastic materials, primarily lapilli and scoria, intercalated with layers of ash containing carbonate and sulphate crusts. With a height reaching 200 m and slope angles ranging between 30° and 35°, the cone exhibits significant fractures that facilitate gas release. The results from stability analyses conducted under unsaturated conditions revealed a factor of safety (F.S., the ratio of stabilizing to destabilizing forces acting on the slope) of around 1.2. However, under saturated conditions, the F.S. drops below 1.0, indicating potential instability during heavy rainfall. Historical rainfall data for the region suggest that heavy rainfall events (>100 mm) occurring within a few hours have a return period of approximately 10 years, and extraordinary rainfall events (>400 mm) accumulating over a short period have a return period of around 50 years. Reaching or exceeding these precipitation thresholds could lead to saturation and instability conditions of the volcanic materials, potentially resulting in lahars originating from the ash and lapilli deposits (Figure 24, left).

Given the possibility of lahars and instability of the slopes of the volcanic cone, the following preventive measures have been proposed:

- Monitoring volcano slope displacements.
- Installation of meteorological stations in the area for early detection of heavy rains.
- Include in the canalization and drainage projects the possibility of intense rainfall with transportation of ashes and other solid materials.

5.6.4. Ground Collapse Risks

Cavities and volcanic caves within lava flows, mainly in pahoehoe lavas, pose a significant hazard of ground collapse, particularly due to overloads from infrastructure foundations which could affect the stability of cavities located at shallow depths beneath excavated ground or beneath infrastructure and foundations. In response to this hazard of ground collapse, the following preventive measures have been proposed:

- Detailed mapping to identify the locations of volcanic caves and cavities.
- Geotechnical borehole investigations and geophysical profiling using ground-penetrating radar to detect cavities in susceptible areas or areas where infrastructure works, excavations, or foundations are planned.

6. Discussion

The volcanic eruption of Cumbre Vieja, La Palma 2021, was the most important and devastating urban eruption of the last 100 years in Europe. Over 1.2 billion euros were spent on reconstruction projects and aid to minimize the social and economic impacts. These projects were planned on the lava flows, with the objective of starting works in less than 1 year after the eruption for roads, and between 2 and 3 years for other types of projects. However, the estimated cooling times for the lava flows have been estimated to be more than 5 years, which was not acceptable for project timelines.

In order to provide feasible solutions to initiate reconstruction in the shortest possible timeframe, thermal, geological, and geotechnical investigations were conducted with the objective of calculating the cooling rates of the lava flows and hence the time required to reach acceptable temperatures, as well as their thermal and geomechanical properties. The results from in situ investigations have enabled the estimation of cooling times through the development of two ad hoc models, namely the homogeneous and heterogeneous models. In the former, lava flows were considered as a physical element exhibiting isotropic and homogeneous behavior, while in the latter model, their behavior was characterized as anisotropic and heterogeneous. In both models, data from four boreholes drilling on aa and pahoehoe lavas up to a depth of 10.5 m have been utilized.

The systematic recording of temperatures measured at surface and in the boreholes at various depths during the period between August 2022 and November 2023 has enabled comparison between the measured in situ temperatures and those estimated from the models (Section 4.5), yielding maximum deviations of 12.8% for the homogeneous model and 16.3% for the heterogeneous model, with temperatures being overestimated by both models.

Although the homogeneous model yielded smaller deviations, the heterogeneous model is more representative of the actual conditions of the lava flows. Additionally, the majority of the data from the boreholes correspond to aa lavas, with a smaller proportion pertaining to pahoehoe lavas, which may result in less representative results for pahoehoe lavas. On the other hand, the homogeneous model cannot be extrapolated to other locations, unlike the heterogeneous model. This is because the homogeneous model requires periodic temperature measurements from a specific site, whereas the heterogeneous model needs information regarding the lithological composition and thickness of various materials, typically acquired through borehole drilling, to estimate cooling times.

The lava flows' cooling times provided by the models to reach temperatures below 50 °C at depths less than 10 m have averaged 5 years. However, the deadlines to initiate reconstruction were less than 3 years, and even less than 1 year for roads. Consequently, to meet the requirements, two possible solutions based on the thermal behavior of the lava flows to achieve temperatures between 30 °C and 50 °C, compatible with reconstruction activities and within shorter timeframes, were studied.

The first solution was based on avoiding excavation of the upper scoriaceous crust of the lava flow, which has relatively low thermal conductivity. This crust would act as an insulating material compared to the basaltic inner core of the lava flow, which has relatively high thermal conductivity. In this way, the infrastructure should rest on the surface of the lava flow, duly conditioned for the type of construction in question (road, foundation). This thermal behavior of the lava flows was experimentally verified during the construction of new roads by measuring temperatures on the surface of the lava flows. In areas where the upper scoriaceous crust was excavated, these temperatures were compared with those measured in areas around 20 m away from the road where the upper scoriaceous crust was not excavated. The results obtained consistently showed much lower temperatures where the upper crust of the lava flow had not been excavated (Figures 17 and 18). The application of this solution to the construction of new roads would allow to start the works before 1 year after the eruption.

The second and complementary solution involved constructing a low-thermal-conductivity soil fill on the surface of the lava flow, so that this fill would act as an insulating element. The thickness of soil needed to achieve surface temperatures on the lava flows compatible

with the type of activity was calculated; for agricultural recovery purposes, the soil fill thickness was calculated between 1.5 and 2.5 m, to reach a surface compatible temperature of 30 °C (Section 5.3).

In Hawaii, it has been found that breaking down the size of lava fragments promotes fertility and results in improved water storage capacity. Thus, mechanical preparation of ground for planting is also critical.

The volcanic eruption of Cumbre Vieja in 2021 has resulted in a significant geomorphological transformation of the landscape, with the emission of large volumes of lava flows and pyroclastic materials, in addition to the formation of a large volcanic cone. These new lava deposits could give rise to potential geohazards, including ground subsidence due to collapses of cavities or lava tubes, instability and failure of the volcanic cone slopes, ash and pyroclasts lahars in the event of very heavy rains, and the emission of toxic gases.

Some of these hazards are contingent upon very intense precipitation events, being of low probability, although historical records confirm this possibility. In response, certain prevention measures have been proposed to avoid geohazards and mitigate possible consequences. Preventive measures have been taken by evacuating the affected population and installing a permanent system for monitoring gas emissions.

La Palma Island has a twin sister volcanic island in the middle of the Pacific Ocean, 12,000 km to the west. Like La Palma, Hawaii Island's economy is based on tourism and agriculture, and both islands are noted for their astronomical observatories. Although more voluminous and more geochemically complex [29], the 2018 eruption of Kilauea volcano [30] was very similar to La Palma's 2021 eruption, devastating agricultural lands with 36 km^2 of basalt lava, destroying over 700 structures, and covering more than 50 km of paved roads [31]. Reconstruction of major roads over lava flows with thicknesses in excess of 25 m was an economic priority, but surface lava temperatures in excess of 400 °C damaged equipment and hindered re-paving. Cooperative discussions between Hawaiian and Spanish engineers and geologists about road reconstruction were useful, and the La Palma engineering studies will be beneficial to lava flow recovery in other volcanic areas world-wide.

7. Conclusions

- Two models of lava flow cooling rate have been developed considering the lava as either homogeneous or heterogeneous. The models have been applied to the lava flows of the La Palma 2021 volcanic eruption, based on temperatures measured at different depths, and thermal properties, lithological composition, and thicknesses of the lava flows.
- Both models have allowed calculation of cooling times of the lava flows, and the results have been verified by comparing the temperatures estimated by the models with those instrumentally recorded in situ. The maximum deviations obtained were 12% for the homogeneous model and 16% for the heterogeneous model.
- Two types of solutions based on the thermal behavior of lava flows have been proposed, aiming to expedite the reconstruction of areas covered by the eruption materials within significantly shorter timeframes than those estimated by cooling models, and at temperatures compatible with infrastructure reconstruction and agricultural recovery. These solutions have been experimentally verified in excavations carried out for the construction of new roads.
- The lava flow cooling models and the proposed solutions based on thermal behavior of lava flows could be applicable to future eruptions in the Canary Islands, which would allow a more efficient approach to the reconstruction and recovery of the areas affected by lava flows in a shorter period of time.
- Could these solutions be applicable to other volcanic regions? Depending on the type of eruption and the materials emitted, they could be applied if the lava flows have similar geological characteristics, since the concepts and methodologies underlying the cooling models and the thermal behavior of the lava flows are generally applicable.

As a final conclusion, some practical experiences from the La Palma eruption were obtained:

- The reconstruction of new roads over hot lavas may be feasible in the short to medium term after the eruption, making it possible to connect towns and provide essential services.
- The construction of new urban settlements on lava flows is potentially possible in the medium term.
- Thermo–geological–geotechnical knowledge is a key factor for post-eruption reconstruction, planning, and design in volcanic regions, minimizing the consequences of the catastrophe, and providing a positive impact ensuring the safety on the affected population.
- The lessons learned from the La Palma eruption may be applicable to other volcanic regions with similar eruptive processes and social and demographic conditions.

Author Contributions: Coordination: L.G.-d.-V. and N.M.P.; conceptual, methodology, manuscript writing and revision: L.G.-d.-V., A.Á.-H., M.F. and J.P.L.; physical and geological cooling models: A.Á.-H., L.G.-d.-V. and M.F.; geomechanical and geotechnical site investigations: A.M.-H., L.E.H.-G., L.G.-d.-V., J.A.R.-L. and J.P.-P.; temperature measurements: P.A.H., D.A.-F. and H.d.-l.-R.; geographic information systems (GISs) and mapping applications: D.A.-F., H.d.-l.-R. and J.P.-P.; geohazards: L.G.-d.-V., A.M.-H., L.E.H.-G., N.M.P. and P.A.H.; territorial recovery and engineering applications: L.G.-d.-V., A.Á.-H. and L.E.H.-G.; resources and management: N.M.P. and L.E.H.-G. All authors have read and agreed to the published version of the manuscript.

Funding: This research was supported by the projects "Recuperación Territorial La Palma" and "LP Agricultura" (Doc. nº 08zu4RDNfd2rsBXk2n5MalbMK_QLVySiG and 0gA9vJOeQiqk-N5Znt31B75_D2U3Y4CPu) financed by Canary Islands' Autonomous Government through the Department of Ecological Transition, Fight Against Climate Change and Territorial Planning, and the General Directorate of Agriculture, respectively.

Data Availability Statement: The temperature data measured in boreholes and on the surface of the lava flows cited in the paper would be available upon formal request to aalvarez@involcan.org.

Acknowledgments: The authors are grateful to David Yamamoto (Hawaii County Department of Public Works), Matt Patrick (USGS Hawaiian Volcano Observatory), and Richelle Takara (Hawaii Department of Transportation). They provided valuable perspectives on the 2018–2020 road construction efforts being applied to the La Palma 2021 volcanic eruption reconstruction. They are also thankful to Rafael Daranas-Carballo (GESPLAN, Canary Islands' Autonomous Government) for his cooperation during La Palma reconstruction projects sharing interdisciplinary information and territorial planning criteria; to José-Heriberto Lorenzo (Caldera de Taburiente National Park) for conducting field trips to identify torrential flood deposits; and to Nestor Rodríguez Santana (Labetec Ingeniería y Control de Calidad), Las Palmas de Gran Canaria) for sharing information on volcanic rocks thermal properties. The authors acknowledge the collaboration of Antonio Álvarez (Toni), Ernaud de Villepreux, Germán Cervigón, José Luis Angulo Santana, Laura Trujillo Vargas, Victor Ortega, and Andrea Alonso González, all linked to INVOLCAN, for their collaboration during the field survey and graphical data processing. The authors wish to express their gratitude to the reviewers for their valuable contributions and suggestions, as well as to the editorial team for their outstanding work; all have undoubtedly contributed to improving the paper. Our sincere thanks to all.

Conflicts of Interest: The authors declare no conflicts of interest.

Appendix A. Geophysical Equipment Used in the Surveys

Table A1. Volcanic cone: MASW seismic, Rayleigh transverse wave analysis with roll along extension.

Equipment		Technical Specifications	
Instrumentation	GEODE de 24 BITS	Number of geophones	12
Manufacturer	Geometrics®	Depth of penetration	30 m
Seismic method	MASW (Rayleigh Wave)	Measurement mode	Roll-along

Table A2. Pahoehoe lava flows: Electromagnetic reflection using Georadar.

Equipment		Technical Specifications	
Instrumentation	IDS Geo-radar	Modulated frequency range	200–600 MHz
Manufacturer	IDS ®	Penetration depth	2 m
Radar technology	Continuous wave SFCW	Measurement mode	In-line

Appendix B. Calculation of the Cooling Factor (CF)

The following procedure has been followed to obtain Equation (16):

$$CF = CRC^n \cdot f(TR) \tag{A1}$$

CF depends on a power of CRC and f (TR), which in turn depends only on TR. The form chosen for this function would be that of a first-degree polynomial, in which it has been taken into account that it is bounded between the values 0 and 1 (so that CF itself does not exceed these limits), and to analyze the theoretical behavior associated with the TR. The definition of this function is:

$$f(TR) = a \cdot TR + b; TR \in [0,1] \bigwedge 0 \leq f(TR) \leq 1^{(*)} \tag{A2}$$

(*) $\bigwedge$ is expressed as and in mathematical terms

Since it has the form of a straight line, the parameter a is the slope, and b the origin point. On the other hand, since it is required that the greater the TR the smaller the CF, likewise, the greater the TR the smaller value of f (TR), and for this purpose, the slope should be negative (a < 0). Furthermore, the minimum value of TR would have to be assigned to the maximum value of the function:

$$f(TR = 0) = 1 \tag{A3}$$

$$f(TR = 0) = a \cdot 0 + b = 1 \rightarrow b = 1 \tag{A4}$$

$$0 \leq f(TR) \leq 1 \rightarrow 0 \leq b \cdot TR + 1 \leq 1 \tag{A5}$$

Since the minimum is reached with TR = 1, this would be the value to obtain the validity interval of the slope:

$$\begin{cases} 0 \leq a \cdot 1 + 1 \\ a \cdot 1 + 1 \leq 1 \end{cases} \tag{A6}$$

$$\begin{cases} a \geq -1 \\ a \leq 0 \end{cases} \rightarrow -1 \leq a \leq 0 \tag{A7}$$

From this procedure, we have been able to determine the ordinate at the origin and the limiting values of the slope of f (TR). However, a priori we do not have more information based on physical implications that allow us to find the specific value of the slope, as well as the power of CRC (n), so we will start from mathematical implications to be able to do so. In order to estimate these two values, it has been decided to start from the concept of correlation coefficient, which can be used to estimate how good a linear fit has been from a set of data distributed in a plane (x, y). Specifically, the plane in this case will be made up of the two variables with which the heterogeneous model is to be carried out: the cooling coefficient (λ) and CF. In this way, the correlation coefficient will be evaluated for the values collected in the validity interval of a, and assuming the same validity interval for n, choosing as valid those values that present the maximum correlation value (Figure A1). Since it is a question of solving a problem in an approximate way, values for both parameters will be swept within the limits of each one (in this case, a step of 0.01 has been chosen for both).

Following this procedure, a correlation of 0.9797 was obtained, and the following values were found for the parameters a and n:

$$a = -0.55 \pm 0.01$$

$$n = 0.32 \pm 0.01$$

Resulting in the following expression for CF:

$$CF = CRC^{0.32 \pm 0.01} \cdot [1 - (0.55 \pm 0.01) \cdot TR] \quad \text{(A8)}$$

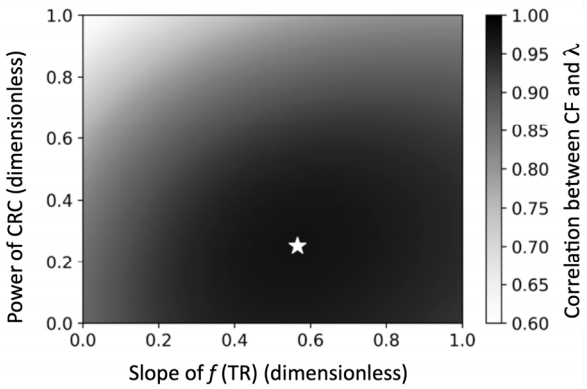

Figure A1. Representation of the correlation matrix between λ and CF. ☆: maximum correlation value.

References

1. Klügel, A.; Schmincke, H.U.; White, J.D.L.; Hoernle, K.A. Chronology and volcanology of the 1949 multi-vent rift-zone eruption on La Palma (Canary Islands). *J. Volcanol. Geotherm. Res.* **1999**, *94*, 267–282. [CrossRef]
2. Carracedo, J.C.; Badiola, E.R.; Guillou, H.; de La Nuez, J.; Torrado, F.P. Geology and volcanology of la Palma and El Hierro, western Canaries. *Estud. Geológicos* **2001**, *57*, 175–273. [CrossRef]
3. Klügel, A.; Galipp, K.; Hoernle, K.; Hauff, F.; Groom, S. Geochemical and volcanological evolution of La Palma, Canary Islands. *J. Petrol.* **2017**, *58*, 1227–1248. [CrossRef]
4. Carracedo, J.C.; Troll, V.R.; Day, J.M.D.; Geiger, H.; Aulinas, M.; Soler, V.; Deegan, F.M.; Perez-Torrado, F.J.; Gisbert, G.; Gazel, E.; et al. The 2021 eruption of the Cumbre Vieja volcanic ridge on La Palma, Canary Islands. *Geol. Today* **2022**, *38*, 94–107. [CrossRef]
5. Milford, C.; Torres, C.; Vilches, J.; Gossman, A.; Weis, F.; Suárez-Molina, D.; García, O.E.; Prats, N.; Barreto, Á.; García, R.D.; et al. Impact of the 2021 La Palma volcanic eruption on air quality: Insights from a multidisciplinary approach. *Sci. Total Environ.* **2023**, *869*, 161652. [CrossRef]
6. Reyes-Hardy, M.P.; Biass, S.; Domínguez, L.; Di Maio, L.S.; Frischknecht, C.; Bonadonna, C.; Pérez, N. Temporal evolution of roof collapse from tephra fallout during the 2021-Tajogaite eruption (La Palma, Spain). *Front. Earth Sci.* **2023**, *11*, 17. [CrossRef]
7. Hirashima, K. Rate of cooling of lava flows. In Proceedings of the Thirty-First Annual Meeting of the Highway Research Board, Washington, DC, USA, 15–18 January 1952; Volume 31.
8. Suto, S.; Sakaguchi, K.; Matsubayashi, O.; Kamata, H.; Katoh, K.; Yamamoto, T. Temperature measurement of lava of 1983 in Miyake-jima, May 1985. In *Report of Coordinating Committee for Prediction of Volcanic Eruptions*; Japan Meteorological Agency: Tokyo, Japan, 1985; Volume 34, pp. 15–17.
9. Suto, S.; Yamamoto, T. Cooling history of the lava of 1983, Miyake-jima, in these three years with the formation of the hydrothermal system. *J. Geotherm. Res. Soc. Jpn.* **1988**, *10*, 211–224. [CrossRef]
10. Patrick, M.R.; Dehn, J.; Dean, K. Numerical modelling of lava flow cooling applied to the 1997 Okmok eruption: Approach and analysis. *J. Geophys. Res. Solid Earth* **2004**, *109-B3*, B03202. [CrossRef]
11. Davies, A.G.; Matson, D.L.; Veeder, G.J.; Johnson, T.V.; Blaney, D.L. Post-solidification cooling and the age of Io's lava flows. *Icarus* **2005**, *176*, 123–137. [CrossRef]
12. von Aulock, F.W.; Ferk, A.; Leonhardt, R.; Hess, K.U.; Cordonnier, B.; Dingwell, D.B. The influence of cooling rates on the paleointensities of volcanic glasses tested on synthetic and natural glass. In *Proceedings of the AGU Spring Meeting Abstracts*; AGU, Toronto, Canada, December-2008, 2009; GP11C-04. Available online: https://www.researchgate.net/publication/260688646_The_Influence_of_Cooling_Rates_on_the_Paleointensities_of_Volcanic_Glasses_Tested_on_Synthetic_and_Natural_Glass (accessed on 9 January 2024).
13. Basu, D.; Das, K.; Self, S. *Numerical Simulation and Analysis of Lava Flow Cooling*; Contract NERC-02-07-006; US Nuclear Regulatory Commission: Washington, DC, USA, 2012; 40p.

14. Willians, R.S. *Lava-Colling Operations during the 1973 Eruption of Eldfell Volcano, Heimaey Vestmannaeyjar, Iceland*; U.S. Geological Survey Open-File Report 97-724; USGS: Woods Hole, MA, USA, 2013; 74p. Available online: https://pubs.usgs.gov/of/1997/0724/report.pdf (accessed on 9 January 2024).
15. Harris, A.J.; Rowland, S. FLOWGO: A kinematic thermo-rheological model for lava flowing in a channel. *Bull. Volcanol.* **2001**, *63*, 20–44. [CrossRef]
16. Harris, A.; Bailey, J.; Calvari, S.; Dehn, J. Heat loss measured at a lava channel and its implications for down-channel cooling and rheology. In *Kinematics and Dynamics of Lava Flows*, Manga, M., Ventura, G., Eds.; Geological Society of America Special Paper 396; GSA. 2005, pp. 125–146. Available online: https://www.ldeo.columbia.edu/~ruprecht/Site/Classes_files/Week7_Harris.pdf (accessed on 28 February 2024).
17. Neri, A. A local heat transfer analysis of lava cooling in the atmosphere: Application to thermal diffusion-dominated lava flows. *J. Volcanol. Geotherm. Res.* **1998**, *81*, 215–243. [CrossRef]
18. Gobierno de España; Gobierno de Canarias; Cabildo de La Palma; Ayuntamiento de Los Llanos de Aridane; Ayuntamiento de El Paso; Ayuntamiento de Tazacorte. *Informe Sobre las Actuaciones y Medidas Emprendidas tras la Erupción del Volcán de Cumbre Vieja (La Palma), Seis Meses Después del Inicio de la Emergencia*; Comisión Mixta Para la Reconstrucción, Recuperación y Apoyo a la Isla de La Palma: La Palma, Spain, 2022. (In Spanish)
19. Newhall, C.; Self, S. The Volcanic Explosivity Index (VEI): An estimate of explosive magnitude for historical volcanism. *J. Geophys. Res.* **1982**, *87*, 1231–1238. [CrossRef]
20. Bonadonna, C.; Pistolesi, M.; Biass, S.; Voloschina, M.; Romero, J.; Coppola, D.; Folch, A.; D'Auria, L.; Martin-Lorenzo, A.; Dominguez, L.; et al. Physical characterization of long-lasting hybrid eruptions: The 2021 Tajogaite eruption of Cumbre Vieja (La Palma, Canary Islands). *J. Geophys. Res. Solid Earth* **2022**, *127*, e2022JB025302. [CrossRef]
21. Dóniz-Páez, J.; Németh, K.; Becerra-Ramírez, R.; Hernández, W.; Gosálvez, R.U.; Escobar, E.; González, E. Tajogaite 2021 Eruption (La Palma, Canary Islands, Spain): An exceptional volcanic heritage to develop geotourism. *Proceedings* **2023**, *87*, 26. [CrossRef]
22. Self, S.; Keszthelyi, L.; Thordarson, T.H. The importance of pahoehoe. *Annu. Rev. Earth Planet. Sci.* **1998**, *26*, 81–110. [CrossRef]
23. Lockwood, J.P.; Hazlett, R.W.; de la Cruz-Reyna, S. *Volcanoes—Global Perspectives*, 2nd ed.; Wiley-Blackwell: New York, NY, USA; Oxford, UK, 2022; 465p.
24. Flyinn, L.P.; Mouginis-Mark, P.J. Cooling rate of and active Hawaii on lava flow from nighttime spectroradiometer measurements. *Geophys. Res. Lett.* **1992**, *19*, 1783–1786. [CrossRef]
25. Ausfastirama, M.; Hoskuldsson, A.; Jonsadottir, I.; Ulfarsson, M.O. New Insights for Detecting and Deriving Thermal Properties of Lava Flow Using Infrared Satellite during 2014–2015 Effusive Eruption at Holuhraun, Iceland. *Remote Sens.* **2018**, *10*, 151. [CrossRef]
26. Oppenheimer, C. Lava flow cooling estimated from landsat thematic mapper infrared data: Loquimay eruption (Chile, 1998). *J. Geophys. Res.* **1991**, *96*, 21865–21878. [CrossRef]
27. Maruyama, S.; Moriya, S. Newton's law of cooling: Follow up and exploration. *Int. J. Heat Mass Trans.* **2021**, *164*, 120544. [CrossRef]
28. Rodríguez-Santana, N.; (LABETEC Ingeniería y Control de Calidad, Las Palmas de Gran Canaria, Spain). Personal communication, 2022.
29. Gansecki, C.; Lee, R.L.; Shea, T.; Lundblad, S.P.; Hon, K.; Parcheta, C. The tangled tale of Kilauea's 2018 eruption as told by geochemical monitoring. *Science* **2019**, *366*, 6470. [CrossRef]
30. Neal, C.A.; Brantley, S.R.; Antolik, L.; Babb, J.L.; Burgess, M.; Calles, K.; Cappos, M.; Chang, J.C.; Conway, S.; Desmither, L.; et al. The 2018 rift eruption and summit collapse of Kilauea volcano. *Science* **2019**, *363*, 367–374. [CrossRef]
31. Takara, R. Facing volcanic challenges. *Public Roads* **2020**, *84–2*, 26–29. Available online: https://highways.dot.gov/sites/fhwa.dot.gov/files/2021-01/Public%20Roads%20Summer-2020.pdf (accessed on 11 March 2024).